J. Membrane Biol. 90, 67–87 (1986)

The Journal of
Membrane Biology

Generalized Kinetic Analysis of Ion-Driven Cotransport Systems: II. Random Ligand Binding as a Simple Explanation for Non-Michaelian Kinetics

Dale Sanders
Department of Biology, University of York, Heslington, York YO1 5DD, England

Summary. Solute uptake in many cells is characterized by a series of additive Michaelis-Menten functions. Several explanations for these kinetics have been advanced: unstirred layers, transport across more than one membrane, effects of solute concentration on membrane potential, numerous carrier systems. Although each of these explanations might suffice for individual cases, none provides a comprehensive basis for interpretation of the kinetics. The most common mechanism of solute absorption involves cotransport of solute with a driver ion. A model is developed in which solute and driver ion bind randomly to a membrane-bound carrier which provides a single transmembrane pathway for transport. The kinetic properties of the model are explored with particular reference to its capacity to generate additive Michaelian functions for initial rate measurements of isotopic solute influx. In accord with previous analysis of ordered binding models (Sanders, D., Hansen, U.-P., Gradmann, D., Slayman, C.L. (1984) *J. Membrane Biol.* **77**:123), the conventional assumption that transmembrane transit rate-limits transport has not been applied. Random binding carriers can exhibit single or multiple Michaelian kinetics in response to changing substrate concentration. These kinetics include high affinity/low velocity and low affinity/high velocity phases (so-called "dual isotherms") which are commonly observed in plant cells. Other combinations of the Michaelis parameters can result in *cis*-(substrate) inhibition. Despite the generality of the random binding scheme and the complexity of the underlying rate equation, a number of predictive and testable features emerge. If external driver ion concentration is saturating, single Michaelian functions always result and increasing internal substrate concentration causes uncompetitive inhibition of transport. Numerical analysis of the model in conditions thought to resemble those in many experiments demonstrates that small relative differences in a few key component rate constants of the carrier reaction cycle are instrumental in generation of dual isotherms. The random binding model makes the important prediction that the contributions of the two isotherms show opposing dependence on external concentration of driver ion as this approaches saturation. In the one case in which this dependence has been examined experimentally, the model provides a good description of the data. Charge translocation characteristics of the carrier can be determined from steady-state kinetic data on the basis of the response of substrate flux to modulation of internal driver ion concentration. The application of the model to dual isotherm kinetics is discussed in relation to "slip" models of cotransport, in which the carrier is assumed to have the capability to transport substrate alone **or** with the driver ion. A method for distinguishing between the two models is suggested on the basis of measurement of charge/solute transport stoichiometry as a function of external driver ion concentration.

Key Words cotransport · kinetics · reaction kinetic model · dual isotherm · random binding · slip

Introduction

Solute uptake by a variety of plant cells and tissues does not obey simple Michaelis-Menten kinetics. Typically, influx begins to saturate as a function of increasing solute concentration if the solute concentration is maintained below about 100 μM. As the solute concentration is raised beyond this range, influx is further stimulated, and may even fail to saturate at concentrations as high as 100 mM (Epstein, 1976). Lineweaver-Burke plots of such data are concave-downward.

Some early explanations for these complex kinetics favored an interpretation based on transport across two membranes (plasma membrane and tonoplast) in series (Laties, 1969). However, concave-downward Lineweaver-Burke plots are also observed in evacuolate algae (Kannan, 1971), which suggests that the phenomenon is a property of the plasma membrane alone. These observations on unicellular algae (*see also* Komor & Tanner, 1975) and on suspension-cultured or isolated cells of higher plants (Mettler & Leonard, 1979; McDaniel, Lyons & Blackman, 1981; van Bel, Borstlap, van Pinxteren-Bazuine & Ammerlaan, 1982) also militate against generalized interpretations which invoke unstirred layers in the apoplast of multicellular higher plant tissue (Ehwald, Meshcheryakov & Kholodova, 1979).

There have been many attempts to apply a mathematical formalism to the transport kinetic data from plants. Initial work suggested that the curvilinear Lineweaver-Burke plots might result

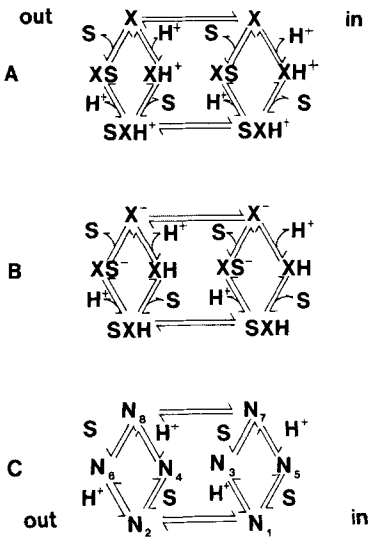

Fig. 1. (*A*) Reaction kinetic scheme for random binding of solute (S) and H^+ to carrier (X) catalyzing cotransport. Carrier is represented as transporting positive charge in the loaded form (RB^+ model). (*B*) As *A*, but with loaded carrier neutral and charge transfer occurring on the unloaded form of the carrier (RB^- model). (*C*) Generalized reaction kinetic scheme for RB^+ and RB^- models. Concentration (density) of carrier state j is designated N_j, with rate constants (not shown) from carrier state i to state j designated k_{ij}

from the operation of two discrete, but additive, saturable systems (Epstein, Rains & Elzam, 1963). More detailed curve fitting revealed that most data could not be described as the sum of two additive Michaelian processes (Nissen, 1974). Instead, it was proposed that kinetic data might be accounted for by the existence of as many as eight separate and nonadditive Michaelian "phases." This suggestion provoked the formulation of a number of models to describe the underlying mechanism of transport (Bange, 1979; Sabater, 1982). However, in a comprehensive and rigorous study, Borstlap (1981, 1983) has shown for several solutes (organic and inorganic) that a markedly simpler algorithm suffices for fitting of all data so far examined. The algorithm comprises three additive phases: two Michaelian and one linear. While it might reasonably be thought that the last of these phases is the result of "passive" diffusion (Borstlap, 1977, 1981), the origin of the other two is not so clear.

The most common mechanism of solute uptake involves cotransport of the solute with one or more driver ions (Eddy, 1978; Poole, 1978; West, 1980; Sanders, 1984). Driver ion influx is thermodynamically downhill and therefore energies the accumulation of solute. Komor and Tanner (1974, 1975) used a reaction kinetic scheme for proton/hexose cotransport to explain the existence of two Michaelian phases for hexose uptake by *Chlorella* and the responses of these phases and of the net hexose-dependent proton influx to changes in external pH. They proposed that the hexose carrier can cross the membrane in one of two loaded forms: with the hexose molecule alone (representing the lower affinity phase), or fully loaded with the hexose and a hydrogen ion (higher affinity). Since the binary carrier-solute complex is capable only of dissipative transport (with respect to the transmembrane electrochemical gradient of solute), dual pathway schemes like this have been termed "slip" models (Eddy, 1980).

One limitation in applicability of the slip model, however, is that it does not account for the observation that in some systems the Michaelian phase with the **lower** affinity can operate **against** the transmembrane electrochemical gradient of solute (e.g. Gerson & Poole, 1972; van Bel et al., 1982; Sanders, 1984). The aim of the present paper is to explore the properties of an alternative (but extremely simple) reaction kinetic model for solute-driver ion cotransport in which the solute and a driver ion bind randomly to a carrier. The model allows only one transmembrane pathway for solute movement (that of the ternary driver ion/solute/carrier complex) and this means that solute transport can be energized by the driver ion gradient under all conditions. It is demonstrated that such models are capable of explaining the two Michaelian phases of plant solute transport. Furthermore, the model is testable with respect to the dependence of transport on the external concentration of driver ion. Preliminary accounts of this work have appeared elsewhere (Sanders & Slayman, 1983; Sanders, 1984).

The Model

General Description and Assumptions

Solute uptake is assumed to be mediated by a carrier (X) whose ligand binding sites are exposed alternately to the outside and inside of the cell. The carrier possesses binding sites for both the solute (S) and a driver ion (H^+). Detailed consideration will be given only to the case in which H^+ and S are transported in a stoichiometric ratio of 1, though the model can easily be extended to incorporate other ratios. Likewise, since the vast majority of cotransport systems operate electrophoretically, transporting positive charge into the cell, treatment will focus on the simplest case in which S bears no net charge and the current is therefore carried by H^+.

It is further assumed that the carrier is able to traverse the membrane in one of only two states: either completely unloaded or fully loaded with S and H^+. This simplification may be justified on the grounds that significant permeability of intermediate states (XS, XH^+) would serve to uncouple the fluxes of the li-

gands and hence impair efficient energy transduction (Turner, 1981). Furthermore, careful studies on the H^+-monosaccharide cotransport system of *Rhodotorula gracilis* have failed to uncover any catalytic activity of the partially-loaded carrier (Neimietz & Höfer, 1984). Results of relaxing this assumption are dealt with in the Discussion. The presence of only one charge-carrying pathway categorizes the transport system as "Class-I." Current-voltage relations of Class-I systems have been explored already by Hansen, Gradmann, Sanders and Slayman (1981).

S and H^+ are considered to bind **randomly** to X. In other words, the order of addition of S and H^+ will be statistically determined both by the reaction constants linking the different loaded states of the carrier and by the ligand concentrations. This constitutes an important deviation from our previous treatment of cotransport (Sanders, Hansen, Gradmann & Slayman, 1984), which considered the properties of carriers that are sterically constrained such as to permit only one binding sequence of S and H^+. For two ligands, four separate ordered-binding models have to be specified to accommodate the different permutations of binding order on the two sides of the membrane. The condition of random binding therefore represents the more general case, since, given appropriate values of the ligand binding reaction constants, the single random binding model can effectively merge with any one of the four cases for ordered binding. The *quid pro quo* of this more comprehensive approach is the greater complexity of the resulting rate equations.

Figure 1*A* is a kinetic scheme depicting random binding of S and H^+ to the recycling carrier. Note that although the binding of either ligand to the carrier might be described by as many as four binding constants, it is envisaged that only one binding site need be involved. Thus two different binding constants could arise from the vectorial orientation of the binding site (inside or outside the cell), and another two from the possible difference in affinity resulting from binding of the carrier to the other ligand. For this model (RB^+), transfer of (positive) charge is represented as occurring on the **loaded** form of the carrier. The corresponding transport system in which (negative) charge is moved on the unloaded carrier (RB^-), the loaded form being neutral, is shown in Fig. 1*B*. Both RB^+ and RB^- models can be represented by the generalized scheme in Fig. 1*C*, in which the carrier state densities are represented as N_j.

In accordance with previous nomenclature (Sanders et al., 1984), reaction constants can, where appropriate, also be rewritten to make ligand concentration explicit as, for example, $k_{86} = k^o_{86}[S]_o$. The effect of membrane potential on the charge-transit reactions can be incorporated in the form of a symmetric Eyring barrier as

$$k_{12} = k^0_{12} \exp(zu/2) \tag{1a}$$

and

$$k_{21} = k^0_{21} \exp(-zu/2) \tag{1b}$$

for the RB^+ model, in which z is the net charge on the carrier during transit, k^0_{12} and k^0_{21} the respective backward and forward reaction constants at zero membrane potential, and u the reduced membrane potential, defined as $F\Delta\psi/RT$ (with $\Delta\psi$ the measured membrane potential difference in volts referenced to the cell exterior, F, R, and T having their usual meanings). The corresponding equations for the RB^- model are

Table 1. Partial expansion of the coefficients for the complete rate equation [Eq. (3)]

Coefficient	*Expanded form*
A	$N \cdot k_{21}[k_{15}(k_{37} + k_{31}) + k_{37}k_{13})$
B	$k^o_{42}k^o_{86}[(k_{62} + k_{68})12KA^o_4 + k_{62}20KA^o_8]$
C	$k^o_{42}(k_{62} + k_{68})52KA_4 + k^o_{86}k_{62}44KA_8$
D	$[k_{15}(k_{37} + k_{31}) + k_{37}k_{13}][(k_{62} + k_{68})(k_{21} + k_{24}) + k_{26}k_{68}] + k_{12}[(k_{37} + k_{31})(k_{24}(k_{62} + k_{68}) + k_{26}k_{68}]$
E	$k^o_{42}k^o_{86}52KA^{oo}_T$
F	$k^o_{42}172KA^o_T + k^o_{86}76KA^o_T$
G	$212KA_T$

$$k_{87} = k^0_{87} \exp(-zu/2) \tag{2a}$$

for the backward direction, and

$$k_{78} = k^0_{78} \exp(zu/2) \tag{2b}$$

for the forward direction.

Isotope Fluxes Through Random Binding Systems

Schemes such as those in Fig. 1 can be treated as conventional enzymic reactions. Hence the formalism developed for description of the kinetic behavior of enzymes can also be applied to random binding carriers in order to derive the complete rate equation describing isotopic flux through the systems. The rate equation is derived in Appendix I by the method of King and Altman (1956) and can be written in the form

$$J_s = \frac{A[S]_o(B[S]_o + C)}{D(E[S]^2_o + F[S]_0 + G)} \tag{3}$$

in which J_s is the flux of isotopic S from outside to inside, $[S]_o$ is external concentration of S, and the coefficients A through G are constants from which $[S]_o$ has been extracted, but which between them comprise various combinations of all the component reaction constants of the carrier cycle. Embedded within the coefficients, therefore, are the six reaction constants in which binding of ligands other than $[S]_o$ are subsumed (i.e., binding of $[H^+]_o$, $[H^+]_i$ and $[S]_i$). For ready reference, partial expansion of the coefficients in terms of the reaction constants is given in Table 1. This expansion is, of course, equally valid for the RB^+ and RB^- models: it is merely the identity of the charge-carrying reactions (k_{12}, k_{21} *versus* k_{78}, k_{87}) which is model-dependent.

Although the major conclusions of this paper can be readily comprehended without a detailed understanding of the methods used to derive the complete rate equation, a brief description of the King-Altman method will enable the meaning of some of the symbols in Table 1 to be more easily appreciated. The rate equation is set up as a product of particular carrier-state densities (which are not known) and associated rate constants. The King-Altman method allows the concentration of any given carrier state (N_j where j can hold a value between 1 and 8: *see* Fig. 1) to be written solely in terms of the rate constants and N. For the kinetic diagrams in Fig. 1, N_j/N is given as the sum of 64 terms,

each term the product of seven different rate constants, while N is simply the sum of all eight N_j's (512 terms). Where N_j and N have been expressed as King-Altman functions, they will be denoted as KA_j and KA_T, respectively. The KA terms of particular interest in the present case are those describing N_4 and N_8—the carrier states which combine with external substrate. An integer prefixing the KA expressions will denote the number of additive terms each contains, since it is convenient to group terms according to common rate constants. Where this has been done and a common rate constant then extracted and written explicitly, an "o" suffix will be added, the number of "o"'s signifying the number of extractions. Examples will be seen in Table 1. In deriving Eq. (3), those rate constants subsuming $[S]_o$ (i.e., k_{42}, k_{86}) have been extracted in this manner. Many of the other explicit appearances of rate constants in the coefficients in Table 1 (including the presence of all terms in D) result from the fact that the rate equation is modified to describe **isotopic** flux.

Simplification of the Rate Equation

It will be apparent that Eq. (3) is extremely unwieldy, containing no fewer than ($512 \times 21 =$) 10,752 separate additive terms in the denominator. Much of the rest of this paper will be devoted to exploring its properties, which under some circumstances are surprisingly specific.

Although much can be accomplished by numerical analysis of the rate equation, in order to understand its behavior in an analytic sense it becomes important to simplify it. One common method for simplification assumes that the transmembrane reactions of the carrier are rate limiting to the operation of the carrier cycle, i.e., that the ligand-binding reactions are in rapid equilibrium (Schultz & Curran, 1970; Heinz, Geck & Wilbrandt, 1972; Page & West, 1981; Turner, 1981). However, as we have discussed previously (Sanders et al., 1984), this procedure has severe limitations, since it imposes on the form of the rate equation a condition which does not appear to be physically realistic. The assumption of rapid equilibrium will therefore not be used here. (It should be noted that none of the qualitative conclusions emerging from this work are compromised by imposing the more restrictive equilibrium binding assumption. This point can be confirmed directly by ignoring all terms in which any of the reaction constants k_{12}, k_{21}, k_{78}, k_{87} appear more than once.)

An alternative and more reliable method of simplification is to analyze the behavior of the equation under conditions in which some of the reaction constants are eliminated by consideration of the prevailing experimental conditions. The particular conditions chosen for detailed analysis are:

(i) $[S]_i = 0$. In perfused giant algae (Sanders & Hansen, 1981) and in membrane vesicle systems (not yet operational for assay of cotransport systems in plants, though well developed for the assay of transport in bacterial and animal systems) it is clearly easy to fix $[S]_i$ to 0. However, in intact cells transport is frequently measured after a period of starvation of the solute in question, in order to derepress (Pall, 1971) or otherwise activate (Sanders, 1980) the transport system. Since this treatment often reduces $[S]_i$ considerably, it appears reasonable under some circumstances to assume that $[S]_i$ approaches zero for an initial rate measurement *in vivo*. This has the effect of reducing k_{73} and k_{51} to 0, and hence eliminating all terms which contain these two reaction constants.

(ii) $\Delta\psi$ negative and saturating. To date, current-voltage (I-V) curves have been described for three H^+/organic solute cotransport systems: glucose and amino acids in *Neurospora* (Hansen & Slayman, 1978; Sanders et al., 1983) and amino acids in *Riccia* (Felle, 1981). For each, the I-V relation within the measurable range recorded within seconds of the introduction of the solute lies **parallel** to the voltage axis, but somewhat negative to it. In order words, despite the fact that the cotransport systems carry current, they are all **voltage-insensitive.** This implies that the voltage-sensitive charge-carrying reactions are not rate limiting to the inwardly directed transport cycle, and thus that only terms containing k_{21} (RB^+ model) or k_{78} (RB^- model) need be considered. [The H^+/K^+ cotransport system of *Neurospora*, which displays a finite conductance during initial rate measurements (M.R. Blatt, *personal communication*) may well be an exception to this trend, since high $[K^+]_i$ confers on the system a rather negative reversal potential around which voltage sensitivity can be anticipated.]

Applying both the above simplifying conditions results in a rate equation whose behavior is more readily understood. For example, the 10,752 terms in the denominator of Eq. (3) reduce to 92 terms in the RB^+ model after joint application of conditions i and ii and appropriate cancelling of common terms in numerator and denominator. Furthermore, the experimental justification offered above indicates that numerical analysis of the simplified rate equation is more likely to approximate to the empirical situation than necessary numerical assumptions (however simple) concerning the full rate equation. It is important to note, however, that although the identities of the coefficients A through G change after simplification (*see* Tables 3 and 4), the overall form of the rate equation is identical with that in Eq. (3).

Results

I. Behavior of the Complete Rate Equation

A. The Complete Rate Equation Predicts Two Additive Michaelis-Menten Functions

If uptake of S can be described as the sum of two apparently independent Michaelian processes, we can write

$$J_S = [S]_o\left[\frac{J^{\mathrm{I}}_{\max}}{K^{\mathrm{I}}_m + [S]_o} + \frac{J^{\mathrm{II}}_{\max}}{K^{\mathrm{II}}_m + [S]_o}\right] \tag{4}$$

in which the superscripts I and II define the two phases, each of which is characterized by a saturating velocity, $J_{\max}$, and a Michaelis constant, K_m. Rearranging Eq. (4)

$$J_S = [S]_o\left[\frac{(J^{\mathrm{I}}_{\max} + J^{\mathrm{II}}_{\max})[S]_o + J^{\mathrm{I}}_{\max}K^{\mathrm{II}}_m + J^{\mathrm{II}}_{\max}K^{\mathrm{I}}_m}{[S]^2_o + (K^{\mathrm{I}}_m + K^{\mathrm{II}}_m)[S]_o + K^{\mathrm{I}}_m K^{\mathrm{II}}_m}\right]. \tag{5}$$

Equation (3), which relates flux of isotope to $[S]_o$ in the random binding models 1A and B, can be rewritten in an identical form to Eq. (5) as

$$J_S = [S]_o\left[\frac{\dfrac{AB}{DE}[S]_o + \dfrac{AC}{DE}}{[S]^2_o + \dfrac{F}{E}[S]_o + \dfrac{G}{E}}\right]. \tag{6}$$

Thus, if H^+ and S bind randomly to a carrier which mediates cotransport, the kinetics of influx of isotopic S with respect to $[S]_o$ can be anticipated as representing the sum of two Michaelis-Menten processes. This point has long been recognized by enzyme kineticists for bi-substrate reactions and has more recently been pointed out in the context of transport by Kotyk (1983). Term-by-term comparison of Eq. (6) with Eq. (5) enables the identities of the four Michaelian parameters to be specified in relation to the coefficients A through G as

$$J^{\mathrm{I}}_{\max} + J^{\mathrm{II}}_{\max} = \frac{AB}{DE} \tag{7}$$

$$J^{\mathrm{I}}_{\max}K^{\mathrm{II}}_m + J^{\mathrm{II}}_{\max}K^{\mathrm{I}}_m = \frac{AC}{DE} \tag{8}$$

$$K^{\mathrm{I}}_m + K^{\mathrm{II}}_m = \frac{F}{E} \tag{9}$$

$$K^{\mathrm{I}}_m K^{\mathrm{II}}_m = \frac{G}{E}. \tag{10}$$

Equations (7) through (10) can be solved simultaneously to yield specific and exact relationships between the Michaelian parameters and the coefficients:

$$K^{\mathrm{I}}_m = \frac{F - \sqrt{F^2 - 4EG}}{2E} \tag{11}$$

$$K^{\mathrm{II}}_m = \frac{F + \sqrt{F^2 - 4EG}}{2E} \tag{12}$$

$$J^{\mathrm{I}}_{\max} = A\left[\frac{2CE - B(F - \sqrt{F^2 - 4EG})}{2DE\sqrt{F^2 - 4EG}}\right] \tag{13}$$

$$J^{\mathrm{II}}_{\max} = A\left[\frac{-2CE + B(F + \sqrt{F^2 - 4EG})}{2DE\sqrt{F^2 - 4EG}}\right]. \tag{14}$$

B. Size-Ordering of the Multipliers Determines the Kinetic Behavior of the Complete Rate Equation

So far, no reference has been made to the relative values of the four Michaelian parameters, which will, of course, determine the specific shape of the influx isotherm. The complete rate equation is extremely versatile in its behavior, and three specific responses are considered here.

1. Discrete High Affinity/Low Velocity and Low Affinity/High Velocity Systems ("Dual Isotherm"). In a vast array of plant cells and tissues, and for a similarly impressive spectrum of solutes, biphasic kinetics of solute uptake conforms to a simple pattern, popularly referred to as a "dual isotherm" (Epstein, 1976). Typically, the values of K_m are widely disparate, being separated by a factor of between 10 and 500 (Borstlap, 1983). The $J_{\max}$'s diverge by a smaller factor of between 1.1 and 20, but in all cases analyzed by Borstlap, the lower $J_{\max}$ is associated with the lower value of K_m. Thus, the kinetics can be resolved into two clearly-defined Michaelian phases. For these cases, then, we can define $K^{\mathrm{II}}_m \gg K^{\mathrm{I}}_m$, and the cumbersome exact solutions [Eqs. (11) through (14)] of Eqs. (7) through (10) can be replaced by

$$K^{\mathrm{I}}_m = \frac{G}{F} \tag{15}$$

$$K^{\mathrm{II}}_m = \frac{F}{E} \tag{16}$$

$$J^{\mathrm{I}}_{\max} = \frac{A(CF - BG)}{D(F^2 - EG)} \tag{17}$$

$$J^{\mathrm{II}}_{\max} = \frac{AF(BF - CE)}{DE(F^2 - EG)}. \tag{18}$$

Thus, from the exact solutions [Eqs. (11)–(14)], the condition $K^{\mathrm{II}}_m \gg K^{\mathrm{I}}_m$ implies $F^2 \gg 4EG$, and the condition $J^{\mathrm{II}}_{\max} > J^{\mathrm{I}}_{\max}$ implies $BF > 2CE$. Equations (17) and (18) can then be replaced by even simpler functions derived from Eqs. (13) and (14):

$$J^{\mathrm{I}}_{\max} = \frac{AC}{DF} \tag{19}$$

$$J^{\mathrm{II}}_{\max} = \frac{A(BF - CE)}{DEF}. \tag{20}$$

A numerical example of a dual isotherm is depicted in Figs. 2 and 3 (solid lines).

2. Single Michaelis-Menten Function. In some conditions, the rate equation, despite being essentially biphasic in character, will describe only a **single** Michaelis-Menten function. Several situations can be envisaged:

(i) If $(G/E) = (C^2/B^2)$ and $BF = 2CE$, then Eq. (6) becomes a single Michaelis-Menten function with $J_{\max} = (AB/DE)$ and $K_m = (C/B)$. These conditions characterize the situation for $K^{\mathrm{I}}_m = K^{\mathrm{II}}_m$, as can readily be seen by substitution into Eqs. (7) through (10). [Another, trivial, condition for which $K^{\mathrm{I}}_m = K^{\mathrm{II}}_m$ is $F^2 = 4EG$ (*see* Eqs. (11) and (12)), though in this case $J^{\mathrm{I}}_{\max} + J^{\mathrm{II}}_{\max} = 0$.]

(ii) If $G = [C(BF - CE)]/B^2$, the reduction of Eq. (6) to a Michaelian form results in $J_{\max} = (AB/DE)$ and $K_m = (BF - CE)/BE = (BG/CE)$. This result can again be derived from Eqs. (7) through (10) by setting one of the $J_{\max}s = 0$. The effect is modelled in Figs. 2 and 3 (dashed lines).

(iii) If C and $F \gg B$ and E, the complete rate equation can behave like a single Michaelis-Menten

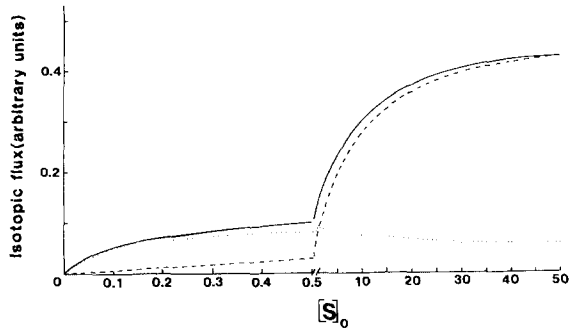

Fig. 2. Three different responses of the generalized rate equation for a random binding carrier [Eq. (3)] to variation of $[S]_o$. Note scale change for $[S]_o > 0.5$. Solid line (——): dual isotherm kinetics with $K_m^{II} \gg K_m^{I}$ and $J_{max}^{II} > J_{max}^{I}$. Values of coefficients: $A = 1$, $B = 5$, $C = 10$, $D = 1$, $E = 10$, $F = 100$, $G = 10$, resulting in the following values for the Michaelis parameters [Eqs. (11)–(14) and Table 2]: $K_m^{I} = 0.10$, $K_m^{II} = 9.90$ (approximate value from Table 2 is 10), $J_{max}^{I} = 0.10$, $J_{max}^{II} = 0.40$. Dashed line (– – – –): Michaelis-Menten kinetics, with $K_m^{I} = K_m^{II}$, based on condition (*ii*) in Table 2. Values of coefficients: as for dual isotherm, except $G = 160$, resulting in the following values for Michaelis parameters [from Eqs. (11)–(14) and Table 2]: $K_m = 8.0$, $J_{max} = 0.5$. Dotted line (·····): *cis*-inhibition kinetics, with $K_m^{II} \gg K_m^{I}$, J_{max}^{II} negative. Values of coefficients: as for dual isotherm, except $B = 0.5$, resulting in values for Michaelis parameters [from Eqs. (11)–(14) and Table 2]: $K_m^{I} = 0.1$, $K_m^{II} = 9.90$, $J_{max}^{I} = 0.1$, $J_{max}^{II} = -0.05$

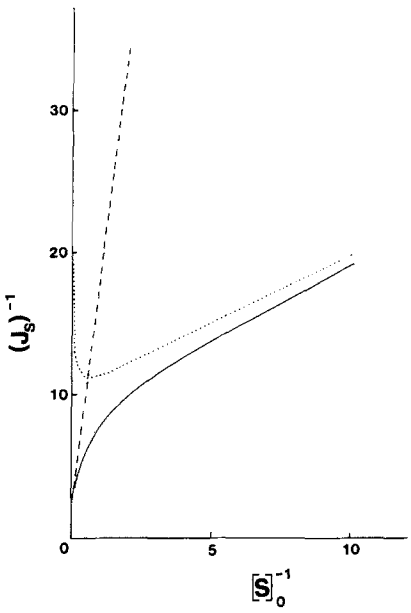

Fig. 3. Double reciprocal plots of the kinetic responses shown in Fig. 2. Solid line (——), dual isotherm; dashed line (– – – –), Michaelis-Menten kinetics; dotted line (·····), *cis*-inhibition

function over a large range of $[S]_o$ because the $[S]_o^2$ terms remain insignificant. Experimentally, this means that one of the two values of K_m is so high as to be unobservable. For that case, the observed K_m is given simply as (G/F). The two values of J_{max} [*see* Eqs. (7) through (9)] reduce to (AC/DF) and $(A[BF - CE]/DEF)$. The latter J_{max}, which will be associated with the very high value of K_m, reduces to 0 with $BF = CE$, so the function then truly describes only a single isotherm. As will be shown later, this is an extremely important condition which may reliably be manipulated in experiments.

3. Cis-Inhibition by S. If the J_{max} associated with the higher value of K_m is negative, flux will tend to decrease as a function of $[S]_o$ over a certain range (which will be determined by the separation of the K_m's). As a specific and simple example, consider the case in which $F^2 \gg 4EG$ (i.e., K_m's are clearly separated), then, as in case i above, the Michaelian parameters are given by Eqs. (15), (16), (19) and (20). J_{max}^{II} will be negative when $CE > BF$. The association of the negative J_{max} with the higher value of K_m (either E or G or both must be much smaller than F, thus K_m^{II} must be greater than K_m^{I}), ensures that the response to flux to $[S]_o$ passes through a clear maximum (Figs. 2 and 3, dotted lines).

A less extreme example of *cis*-inhibition than that shown in Fig. 2 occurs if fluxes in the low concentration range are higher than predicted from Michaelis fits of data at high concentration. These characteristics result if J_{max}^{II} is only slightly negative. Such kinetics have been observed for sulfate transport in the alga *Hydrodictyon* (Rybová, Nešpůrková, Janáček & Stružinský, 1982).

The above discussion is summarized in Table 2.

C. At Saturating $[H^+]_o$, the Complete Rate Equation Always Predicts a Single Michaelis-Menten Function

A central factor in the characterization of the kinetic behavior of the model concerns the response to experimental variables, since this will generate a framework by which its validity might be tested. Although the relationships derived thus far are useful in demonstrating the versatility of the complete rate equation, they give little information on the kinetic response to changes in ligand concentration (other than $[S]_o$) because the rate constants are present in a large number of terms subsumed in each of the **critical** coefficients. [The coefficients A and D are relatively simple but have no determinant role in the generalized kinetic response (*see* Table 2) since they act only as scaling factors for the numerator and denominator of the rate equation.]

$[H^+]_o$ is, of course, one factor which is easy to manipulate experimentally. It enters the overall rate

Table 2. Size ordering of the coefficients in the complete rate equation and generalized kinetic response

Response	Condition	K_m^{I}	K_m^{II}	$J_{\max}^{\mathrm{I}}$	$J_{\max}^{\mathrm{II}}$
Dual isotherm	$F^2 \gg 4EG$; $BF > 2CE$	G/F	F/E	AC/DF	$(A[BF - CE])/DEF$
Michaelis-Menten (i)	$G/E = C^2/B^2$; $BF = 2CE$	C/B	—	AB/DE	—
(ii)	$G = (C[BF - CE])/B^2$	BG/CE	—	AB/DE	—
(iii)	$C, F \gg B, E$; $BF = CE$	G/F	—	AC/DF	—
Cis-inhibition	$F^2 \gg 4EG$; $CE > BF$	G/F	F/E	AC/DF	$(A[BF - CE])/DEF$

equation embedded in the rate constants k_{84} and k_{62}. An important question which can be asked now is: how does saturating $[H^+]_o$ affect the kinetics predicted by Eq. (3)? ("Saturating $[H^+]_o$" is taken to mean that further increases in $[H^+]_o$ have no further effect on transport: other reactions in the kinetic cycle must therefore be rate limiting.) The coefficients can be simplified by expressing each only as a function of those terms in which $[H^+]_o$ is raised to the highest power. They are written below with all forward rate constants for external ligand binding explicit:

$$A = N \cdot k_{21}[k_{15}(k_{37} + k_{31}) + k_{37}k_{13}] \tag{21}$$

$$B = [H^+]_o^2 k_{42}^o k_{86}^o k_{62}^o k_{62}^o [12KA_4^{oo} + 4KA_8^{oo}] \tag{22}$$

$$C = [H^+]_o^3 k_{42}^o k_{84}^o k_{62}^o k_{62}^o [16KA_4^{oo}] \tag{23}$$

$$D = [H^+]_o k_{62}^o \{[k_{21} + k_{24}][k_{15}(k_{37} + k_{31}) + k_{37}k_{13}] + k_{12}k_{24}(k_{37} + k_{31})\} \tag{24}$$

$$E = [H^+]_o k_{42}^o k_{86}^o k_{62}^o [36KA_{\mathrm{T}}^{ooo}] \tag{25}$$

$$F = [H^+]_o^2 k_{42}^o k_{84}^o k_{62}^o [36KA_{\mathrm{T}}^{ooo}] \tag{26}$$

$$G = [H^+]_o^2 k_{84}^o k_{62}^o [16KA_{\mathrm{T}}^{oo}]. \tag{27}$$

Since $[H^+]_o k_{84}^o$ is not present in either of the coefficients B or E, these terms exhibit a smaller power dependence on $[H^+]_o$ than C and F. The former terms therefore make only a negligible contribution to the numerator and denominator, respectively, of the full rate equation. Furthermore, as shown in Appendix II, $BF = CE$: after extraction of the forward rate constants for S_o- and H_o^+-binding, the KA^{00} terms in B are identical with those in C, and those in E identical with those in F. Thus, at saturating $[H^+]_o$, the complete rate equation obeys the size ordering of coefficients necessary for a simple Michaelis-Menten response (*see* Table 2, middle row, example *iii*). Regardless of any detailed variation in the size of the carrier reaction constants, a cotransport system which binds H^+ and S randomly will always exhibit Michaelis-Menten kinetics with respect to S if $[H^+]_o$ is saturating.

This conclusion can also be reached in a non-quantitative manner by considering the nature of random binding, which is essentially a statistical process. As $[H^+]_o$ is raised, the likelihood that H^+ will bind to the carrier before S progressively increases: thus, at saturating $[H^+]_o$, the probability that S will bind last becomes 1 and ligand binding at the external surface is ordered in a statistical (though not in a mechanistic) sense.

D. At Saturating $[H^+]_o$, Increase in $[S]_i$ Inhibits Flux Uncompetitively

In some circumstances, it may be possible to explore the effects of internal ligand concentration on the kinetics of transport (Sanders & Hansen, 1981). In the previous general treatment of the kinetics of ordered binding cotransport systems, it was stressed that such experiments are unlikely to yield much information on the underlying characteristics of the transport system unless conditions are fixed to simplify the complete rate equation. The same principle holds also for random binding systems: the complete rate equation predicts that raising $[H^+]_i$ or $[S]_i$ can result in competitive, noncompetitive or uncompetitive inhibition of transport. However, under the mathematically more restricted—but experimentally attainable—conditions of saturating $[H^+]_o$ a different picture emerges.

For saturating $[H^+]_o$, $J_{\max}$ can, as discussed above, be written as AC/DF and K_m as G/F, with the gross rate constants defined as in Eqs. (3), (21)–(27) and Appendix II. Hence, the ratio $J_{\max}/K_m$ can be described as AC/DG. Since the KA^{oo} terms in Eqs. (23) and (27) are identical (Appendix II), we can write

$$\frac{J_{\max}}{K_m} = \frac{N \cdot k_{42}^o k_{21}[k_{15}(k_{37} + k_{31}) + k_{37}k_{13}]}{[k_{21} + k_{24}][k_{15}(k_{37} + k_{31}) + k_{37}k_{13}] + k_{12}k_{24}(k_{37} + k_{31})}. \tag{28}$$

This relationship is remarkable in being independent of the reaction constants k_{73} and k_{51} which subsume $[S]_i$. Thus, although K_m and $J_{\max}$ might each be sensitive to variation of $[S]_i$ (C, F and G all contain terms exhibiting first- and second-order dependence on $[S]_i$—*see* Appendix II) the ratio between them is fixed. Lineweaver-Burke plots at different

Table 3. Complete expansion of the coefficients [Eq. (3)] for the RB^+ model: $\Delta\psi$ negative, saturating and $[S]_i = 0$

A	$N \cdot k_{57}k_{78}\alpha$
B	$k^o_{42}k^o_{86}k_{62}$
C	$k^o_{42}k_{84}(k_{62} + k_{68}) + k^o_{86}k_{62}k_{48}$
D	1
E	$k^o_{42}k^o_{86}[\alpha\gamma + k_{62}k_{78}\beta]$
F	$k^o_{42}[k_{62} + k_{68}]\{\alpha[(k_{75} + k_{57})(k_{87} + k_{84}) + k_{57}k_{78}] + k_{78}k_{84}\beta\}$ $+ k^o_{86}k_{48}[\alpha\gamma + k_{62}k_{78}\beta]$
G	$\alpha[k_{62} + k_{68}][k_{57}k_{78}(k_{84} + k_{48}) + k_{48}k_{87}(k_{75} + k_{57})]$
with	
α	$k_{15}(k_{37} + k_{31}) + k_{13}k_{37}$
β	$(k_{15} + k_{57})(k_{31} + k_{37}) + k_{13}k_{57}$
γ	$k_{57}(k_{62} + k_{78}) + k_{62}k_{75}$

$[S]_i$ must be parallel if $[S]_i$ has an effect on the flux in these conditions. Thus, if the action of raised $[S]_i$ is to inhibit isotopic influx, **$[S]_i$ can behave only as an uncompetitive inhibitor of isotopic transport of S through a random binding cotransport system at saturating $[H^+]_o$.** (If rate limitation of transport occurs through carrier recycling and exchange diffusion is the primary mode of entry of $^*S$, then S_i will stimulate the flux, but again only through parallel effects on J_{max} and K_m.) Since random binding becomes operationally ordered at saturating $[H^+]_o$, it must be expected that models constrained at the outset to the external binding order H^+ then S should also exhibit uncompetitive kinetics with respect to $[S]_i$. This, indeed, is the case, demonstrated by Eqs. (27) and (28) in Sanders et al. (1984).

In contrast to the specific effects of $[S]_i$ at saturating $[H^+]_o$, variation of $[H^+]_i$ can result in a variety of different classes of kinetic inhibition unless membrane potential is also saturating in the RB^+ model (in which case uncompetitive inhibition is again observed). This can be appreciated with reference to Eq. (28): $H_i k^o_{31}$ is present in the ratio J_{max}/K_m, and has the capacity to decrease this ratio. If k_{21} is dominant ($\Delta\psi$ very negative) $H_i k^o_{31}$-containing terms in numerator and denominator cancel. The discrimination between the effects of S_i and H^+_i might appear surprising at first, since the random binding model looks symmetric for all ligands. However, it has to be recalled that the complete rate equation describes influx of **isotopic** S, and it is the conversion of the King-Altman equation to express this fact that introduces nonequivalent responses of flux to the two ligands (*see* Appendix I).

II. Realistic Biological Simplification of the Complete Rate Equation: $\Delta\psi$ Saturating and $[S]_i = 0$

The aim of exploring the properties of simplified models is twofold. First, since the prevailing practical conditions often approximate to saturating $\Delta\psi$ and $[S]_i = 0$, it is necessary to ensure that the resulting mathematical simplification does not restrict the random binding model from exhibiting some of its important properties outlined above. Second, if it can be shown that the properties of the model do not change considerably after imposition of the more realistic conditions, the simpler expansions of the coefficients A through G enable critical rate constants to be identified as controlling the overall kinetic response of the transport system. Justification of the choice of these particular simplyfing conditions is given in the "Model" section. The condition that $\Delta\psi$ is saturating necessitates that we distinguish between the RB^+ and RB^- models, since the dominant rate constant in the former case is k_{21}, and in the latter it is k_{78}.

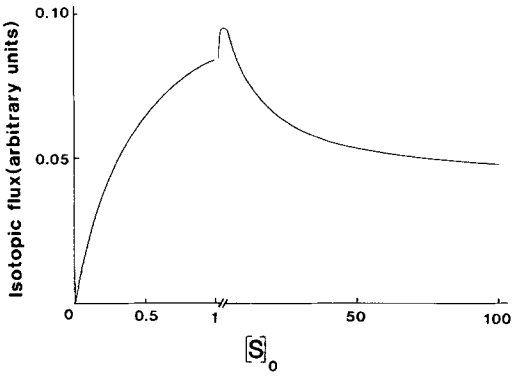

Fig. 4. Specific numerical example of *cis*-inhibition for RB^- model, with $[S]_i = 0$ and $\Delta\psi$ very negative. Note scale change for $[S]_o > 1$. Rate constants were all set to unity except $k_{62} = 0.05$; coefficients in Table 3 were then calculated and these substituted into Eq. (3). Values of Michaelis parameters, from Eqs. (11)–(14) (with approximate values from definitions in Table 2 in brackets): $K^I_m = 0.51$ (0.51), $K^{II}_m = 6.92$ (6.97), $J^I_{max} = 0.13$ (0.14), $J^{II}_{max} = -0.09$ (−0.10)

A. RB^+ Model

1. *Algebraic Derivation of a Rate Equation.* For the experimental conditions in which $\Delta\psi$ is very negative and $[S]_i = 0$, k_{12}, k_{73} and k_{51} can all be set to 0. The coefficients in Eq. (3) can then be simplified considerably. After factorization and cancelling of common terms in numerator and denominator, the coefficients are described explicitly in terms of the component rate constants as in Table 3.

2. *Numerical Modelling.* In the following examples of numerical modelling, all rate constants are set to unity wherever possible in order to highlight those reaction constants which are instrumental in dictating a particular kinetic response. This strategy is

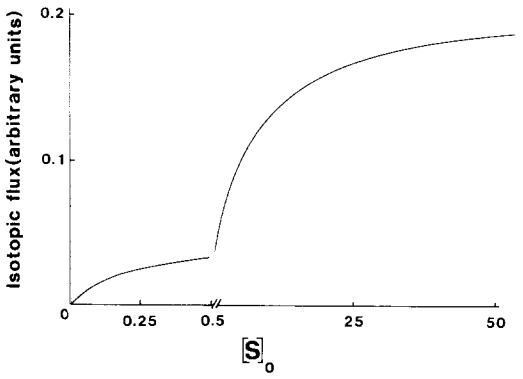

Fig. 5. Specific numerical example of dual isotherm for RB^- model with $[S]_i = 0$ and $\Delta\psi$ very negative. Note scale change for $[S]_o > 0.5$. Rate constants were all set to unity except $k_{68} = k^o_{86} = k_{84} = k_{48} = 0.1$; coefficients in Table 3 were then calculated and these substituted into Eq. (3). Values of Michaelis parameters, from Eqs. (11)–(14) (with approximate values from definitions in Table 2 in brackets): $K^I_m = 0.119$ (0.117), $K^{II}_m = 7.95$ (8.07), $J^I_{max} = 0.030$ (0.029), $J^{II}_{max} = 0.185$ (0.185)

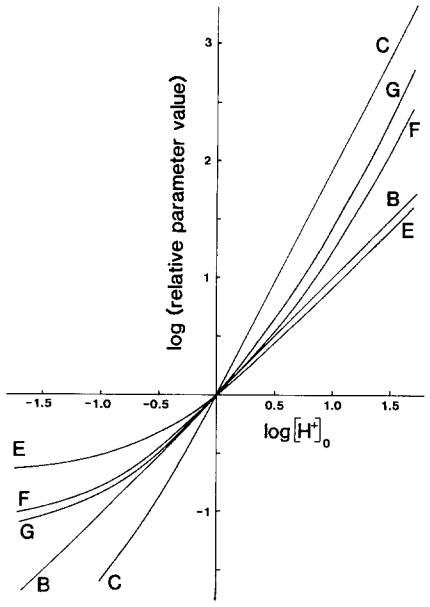

Fig. 6. Response of the coefficients to variation of $[H^+]_o$ for RB^+ model exhibiting dual isotherm kinetics. Multipliers are defined as in Table 3 for the simplifying conditions $[S]_i = 0$ and $\Delta\psi$ very negative. Values for all rate constants as in Fig. 5. Terms A and D are both $[H^+]_o$-insensitive, and are not shown. Reference value of $[H^+]_o = 1$, where $k_{84} = 0.1$ and $k_{62} = 1.0$ (as Fig. 5)

legitimate because the relative, not the absolute, values of the rate constants are the determinant features of the response.

a. Cis-inhibition. The prime condition for *cis*-inhibition (Table 2) is $CE > BF$. Inspection of Table 3 reveals that B can be made very small by setting k_{62} to a low value: the other relevant coefficients all contain k_{62}-independent terms and remain large by contrast. The effect is modelled in Fig. 4 for $k_{62} = 0.05$. This condition implies that at low $[S]_o$, external binding is predominantly in the order H^+-S, while at higher $[S]_o$, S tends to bind first, but transport is impeded by slow binding of H^+ after S.

b. Numerical conditions for dual isotherms. For $K^{II}_m \gg K^I_m$, Table 2 shows that $F^2 \gg 4EG$, and for $J^{II}_{max} > J^I_{max}$, $BF > 2CE$. How can these relationships between the coefficients be obtained with respect to the relative values of the component rate constants? One simple case in which these conditions are fulfilled is illustrated in Fig. 5. There, the non-unity rate constants are $k_{68} = k^o_{86} = k_{84} = k_{48} = 0.1$, which gives $F^2 = 127$, $4GE = 7.4$ and $BF = 1.13$, $2CE = 0.34$, for unity ligand concentrations. This case can be viewed as one of effective positive cooperativity of the transport system: binding of the first ion is not favored, but, once bound, the binding of the second ion is faster. Note, however, that the dissociation constants for both ions, whether binding first or second, are identical. The general simplicity of this case shows that no implausibly complex relations between the individual rate constants need be proposed in order for dual isotherm kinetics to occur.

c. Response of dual isotherm model to change in $[H^+]_o$. Algebraic relations can easily be derived for the J_{max}'s and K_m's by combining the explicit relations in Table 3 with the complete definitions for the Michaelis parameters [Eqs. (11)–(14)]. However, since our purpose here is primarily to examine the feasibility of a random binding explanation for dual isotherms, the response of the specific example shown in Fig. 5 to change in $[H^+]_o$ will be modelled numerically.

Figure 6 shows the response of the coefficients A through G (Table 3) to change in $[H^+]_o$, which is subsumed in k_{84} and k_{62}. Inspection of Table 3 reveals that A and D are $[H^+]_o$-insensitive, while B is linearly dependent on $[H^+]_o$. E contains zero- and first-order terms for $[H^+]_o$ and therefore tends to linear dependence at high $[H^+]_o$. C, F and G all contain both first- and second-order terms, with zero-order terms additionally present in F and G. Thus slopes for C vary between 1 and 2, and for F and G between 0 and 2 for low and high $[H^+]_o$, respectively.

The resultant effects of $[H^+]_o$ on the Michaelis parameters for dual isotherm behavior are shown in Fig. 7. (Note that Figs. 5–8 are modelled for the standard reference condition $[H^+]_o = 1$, with $k^o_{84} = 0.1$ and $k^o_{62} = 1$.) As $[H^+]_o$ is raised, J^{II}_{max} is seen to decrease and K^{II}_m to increase, confirming the predictions of the algebraic analysis of the full model (section IC) in generating a single Michaelis-Menten

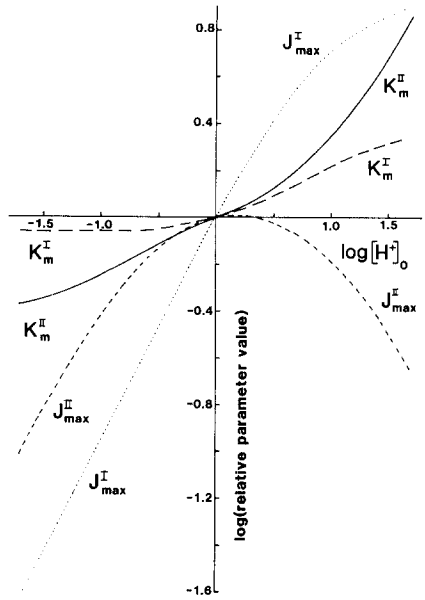

Fig. 7. Effect of $[H^+]_o$ on Michaelis parameters for dual isotherm kinetics: RB$^+$ model. Reference conditions are those of Figs. 5 and 6, with $[H^+]_o = 1$ ($k^o_{84} = 0.1$, $k^o_{62} = 1.0$) and absolute values of rate constants and the Michaelis parameters at $[H^+]_o = 1$ as in the legend of Fig. 5. Michaelis parameters calculated for each $[H^+]_o$ after evaluation of the coefficients in Table 3 and substitution of the coefficients into Eqs. (11)–(14). [Since K_m's are well separated at all $[H^+]_o$, approximate definitions of Michaelis parameters (Eqs. (15), (16), (19), (20) and Table 2) are accurate to within 3% for the whole range of $[H^+]_o$]

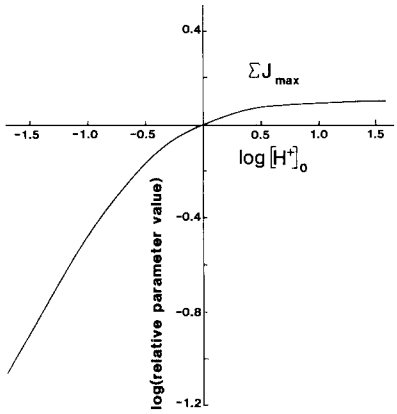

Fig. 8. Response of the isotopic solute flux at saturating $[S]_o$ to variation in $[H^+]_o$ for dual isotherm kinetics: RB$^+$ model. ΣJ_{max} calculated as $J^{I}_{max} + J^{II}_{max}$ from Fig. 7. All conditions as in Fig. 7

function determined by J^{I}_{max} and K^{I}_m. Above the reference $[H^+]_o$, J^{I}_{max} and K^{I}_m both increase, though there is activation of the flux at all $[S]_o$ because J^{I}_{max} is more sensitive than K^{I}_m. Below the reference $[H^+]_o$, J^{I}_{max} and J^{II}_{max} both tend to linear dependence on $[H^+]_o$, with the K_m's becoming insensitive as E, F and G all approach $[H^+]_o$ independence. Dual isotherm kinetics are still observed in this low range of $[H^+]_o$, with the separation of J_{max}'s becoming more marked, and of K_m's less marked, than at the reference $[H^+]_o$.

The dependence on $[H^+]_o$ of the overall $J_{max}(\Sigma J_{max} = J^{I}_{max} + J^{II}_{max})$ is shown in Fig. 8. The decline in J^{II}_{max} at high $[H^+]_o$ is largely compensated for by a corresponding increase in J^{I}_{max}. Thus, ΣJ_{max} increases only 25% as $[H^+]_o$ is raised 50-fold from the reference $[H^+]_o$. (The corresponding increase in J^{I}_{max} is almost eightfold, and the decrease in J^{II}_{max}, fivefold.] This relative insensitivity of ΣJ_{max} to $[H^+]_o$ in the presence of a change in the relative dominance of the two Michaelean phases can be understood as a simple switch in effective binding order of $H^+{}_o$ and S_o, with transport rate-limited primarily by other factors in the carrier reaction cycle. Below the reference $[H^+]_o$, the flux at very high $[S]_o$ tends towards linear dependence on $[H^+]_o$ (Fig. 8), since, of course, J^{I}_{max} and J^{II}_{max} both exhibit linear dependence over this range of $[H^+]_o$ (Fig. 7).

The dependence of ΣJ_{max} on $[H^+]_o$ is, in fact, itself Michaelean and can be written as

$$\Sigma J_{max} = \frac{J_{stim}[H^+]_o}{K_{stim} + [H^+]_o}. \tag{29}$$

This is a general condition for the simplified *RB*$^+$ model (though not for the complete model). Since ΣJ_{max} is defined by Eq. (7) as AB/DE, it can easily be shown from the definitions in Table 3 that

$$J_{stim} = \frac{N\alpha k_{57}k_{78}}{\alpha(k_{57} + k_{75}) + \beta k_{78}} \tag{30}$$

and

$$K_{stim} = \frac{\alpha k_{57}k_{78}}{k^o_{62}[\alpha(k_{57} + k_{75}) + \beta k_{78}]}. \tag{31}$$

For the example in Fig. 8 (with $k^o_{62} = 1$), both J_{stim} and K_{stim} have the value 0.273.

d. Response of dual isotherm model to change in $[H^+]_i$. As with the effects of $[H^+]_o$, the coefficients in Table 3 can be rearranged to show explicitly their behavior with respect to variation of $[H^+]_i$, which is subsumed in the reaction constants k_{31} and k_{75}. The coefficients B, C and D are all independent of $[H^+]_i$, A contains only zero- and first-order terms, while E, F and G all contain zero-, first- and second-order terms. Thus, for dual isotherm conditions, Eqs. (15) and (16) predict that variation of $[H^+]_i$ at high $[H^+]_i$ will have no effect either on K^{I}_m

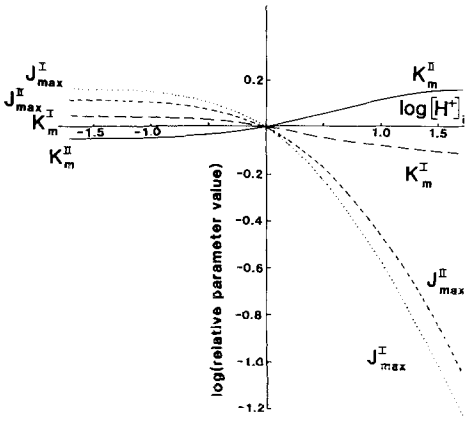

Fig. 9. Effect of $[H^+]_i$ on Michaelis parameters for dual isotherm kinetics: RB^+ model. Reference conditions are those of Fig. 5, with $[H^+]_i = 1$ ($k_{75} = k_{31} = 1.0$) and absolute values of rate constants and the Michaelis parameters at $[H^+]_i = 1$ as in the legend of Fig. 5. Michaelis parameters calculated for each $[H^+]_i$ after evaluation of the coefficients in Table 3 and substitution of the coefficients into Eqs. (11)–(14). [Since K_m's are well separated at all $[H^+]_i$, approximate definitions of Michaelis parameters (Eqs. (15), (16), (19), (20) and Table 2) are accurate to within 3% for the whole range of $[H^+]_o$]

or K^{II}_m. On the other hand, J^{I}_{max} and J^{II}_{max} should both exhibit reciprocal decline as $[H^+]_i$ is raised [*see* Eqs. (19) and (20)]. In other words, $[H^+]_i$ will behave as a noncompetitve inhibitor if $[H^+]_i$ is already high and rate-limiting for transport. A similar conclusion can be derived for the behavior of ordered binding models in which substrate dissociation on the inside occurs before H^+ dissociation (*see* Eqs. (A13) and (A16) in Sanders et al., 1984), but the conclusion does not hold for converse orders of dissociation internally. The random binding model behaves as though dissociation order of S and H^+ inside were constrained because at high $[H^+]_i$ and $[S]_i = 0$, the only source of carrier for combination with H^+_i is that which is not bound to S. The effect is analogous to the behavior of the random binding model at high $[H^+]_o$, where binding also appears to be ordered.

Clearly, however, this noncompetitive inhibition by H^+_i can be guaranteed to occur only if H^+_i terms dominate in the expressions for the K_m's and J_{max}'s. If $[H^+]_i$ is not high, the pattern of inhibition is less well defined. Nevertheless, as shown for the complete model in Section ID, H^+_i will behave as an uncompetitive inhibitor in cases for which $[H^+]_o$ and $\Delta\psi$ are both saturating.

The specific numerical case for which a dual isotherm has been demonstrated (Fig. 5) has also been examined for response to $[H^+]_i$. The results are shown in Fig. 9. The major effect of variation of $[H^+]_i$ is noncompetitive inhibition, even at intermediate concentrations. For the 0.5 unit pH span either side of the pK_a's of the internal H^+ sites (i.e., either side of the control value of $[H^+]_i = 1$), J^{II}_{max} changes by a factor of 1.70, J^{I}_{max} by 2.10, K^{II}_m by 1.22 and K^{I}_m by the factor 1.18. Larger increases in $[H^+]_i$ result, as predicted, in even more marked effects on the J_{max}'s.

Table 4. Complete expansion of the coefficients [Eq. (3)] for the RB^- model: $\Delta\psi$ negative, saturating and $[S]_i = 0$

A	$N \cdot k_{57}k_{21}\alpha$
B	$k^o_{42}k^o_{86}k_{62}[\delta\varepsilon + k_{21}\alpha(k_{62} + k_{68})]$
C	$[k^o_{42}k_{84}(k_{62} + k_{68}) + k^o_{86}k_{62}k_{48}][\delta\varepsilon + k_{21}\alpha(k_{62} + k_{68})]$
D	$\alpha[k_{21}(k_{62} + k_{68}) + \delta] + k_{12}\delta(k_{37} + k_{31})$
E	$k^o_{42}k^o_{86}\{k_{57}[\alpha(k_{62} + k_{26} + k_{21}) + k_{62}((k_{21} + k_{12})(k_{31} + k_{37}) + k_{21}k_{13})] + (k_{37} + k_{31})(k_{26}k_{12}k_{57} + k_{15}k_{21}k_{62})\}$
F	$k^o_{42}\{k_{57}[\alpha((k_{21} + k_{84})(k_{62} + k_{68}) + k_{26}(k_{68} + k_{84})) + k_{84}(k_{68} + k_{62})(k_{21}k_{13} + k_{12}k_{31} + k_{12}k_{37}) + k_{26}k_{12}(k_{37} + k_{31})(k_{84} + k_{68})] + k_{84}k_{21}(k_{15} + k_{57})(k_{37} + k_{31})(k_{68} + k_{62})\}$ $+ k^o_{86}\{k_{57}\alpha[k_{48}(k_{62} + k_{21} + k_{24} + k_{26}) + k_{62}k_{24}] + (k_{31} + k_{37})[k_{57}k_{48}(k_{62}(k_{21} + k_{12}) + k_{12}(k_{24} + k_{26})) + k_{62}(k_{57}k_{24}k_{12} + k_{48}k_{21}k_{15})] + k_{62}k_{48}k_{57}k_{21}k_{13}\}$
G	$k_{57}[k_{48} + k_{84}]\{\alpha[\delta + k_{21}(k_{62} + k_{68})] + k_{12}\delta(k_{37} + k_{31})\}$
with	
α	$k_{15}(k_{37} + k_{31}) + k_{13}k_{37}$
δ	$k_{24}(k_{62} + k_{68}) + k_{68}k_{26}$
ε	$(k_{37} + k_{31})(k_{12} + k_{15}) + k_{37}k_{13}$

B. RB^- Model

1. *Algebraic Derivation of a Rate Equation.* For the case in which charge crosses the membrane on the unloaded carrier and $\Delta\psi$ is very negative, k_{87} can be set to 0 and k_{78} becomes very large. Table 4 shows the simplified definitions of the coefficients in Eq. (3), given this condition and that of $[S]_i = 0$.

2. *Numerical Modelling.*

a. Conditions for dual isotherm. The RB^- model shows dual isotherm kinetics for the same simple conditions chosen for the RB^+ model, namely $k^o_{86} = k_{68} = k_{84} = k_{48} = 0.1$, with all other reaction constants set to 1 (Fig. 10). Values of the Michaelis parameters are given in the figure legend.

b. Response to change in $[H^+]_o$. Figure 11 shows the response to change in $[H^+]_o$ of the Michaelis parameters which describe the dual isotherm condition. Qualitatively, the effect of $[H^+]_o$ is similar to that for the $RB+$ model: J^{II}_{max} passes through a maximum at a pH close to the pK_a of the binding site and behaves reciprocally with respect to $[H^+]_o$ at higher $[H^+]_o$ as the product BF tends to equality with CE. K^{II}_m rises proportionally with

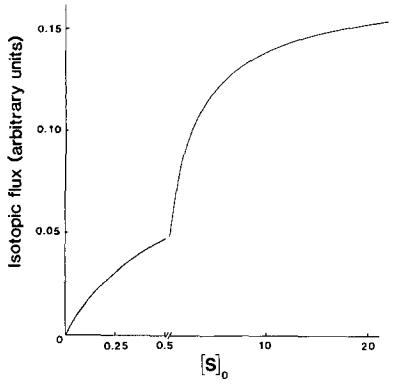

Fig. 10. Specific numerical example of dual isotherm for RB^- model with $[S]_i = 0$ and $\Delta\psi$ very negative. Note scale change for $[S]_o > 0.5$. Rate constants were all set to unity except $k_{68} = k^o_{86} = k_{84} = k_{48} = 0.1$; values for the coefficients in Table 4 were then calculated and these substituted into Eq. (3). Values of Michaelis parameters, from Eqs. (11)–(14) (with values from approximate definitions in Table 2 in brackets): $K^I_m = 0.337$ (0.303), $K^{II}_m = 3.07$ (3.41), $J^I_{max} = 0.053$ (0.059), $J^{II}_{max} = 0.114$ (0.108)

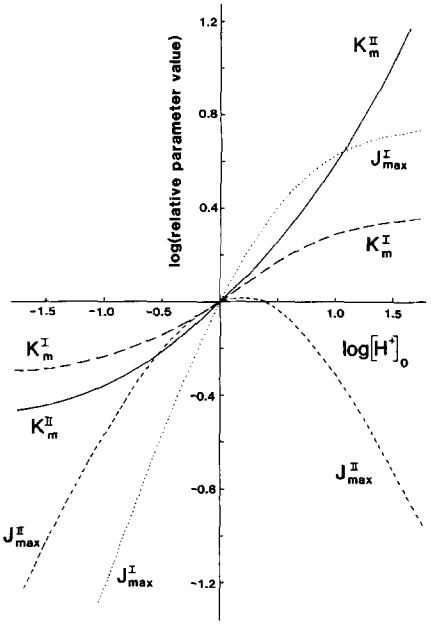

Fig. 11. Effect of $[H^+]_o$ on Michaelis parameters for dual isotherm kinetics: RB^- model. Reference conditions are those of Fig. 10, with $[H^+]_o = 1$ ($k^o_{84} = 0.1$, $k^o_{62} = 1.0$) and absolute values of rate constants and the Michaelis parameters at $[H^+]_o = 1$ as in the legend of Fig. 10. Michaelis parameters calculated for each $[H^+]_o$ after evaluation of the coefficients in Table 4 and substitution of the coefficients into Eqs. (11)–(14)

$[H^+]_o$ over that range, while J^I_{max} and K^I_m both start to saturate. If $[H^+]_o$ is rate limiting, both J_{max}'s tend to shown proportionality with $[H^+]_o$, while both K_m's are relatively insensitive.

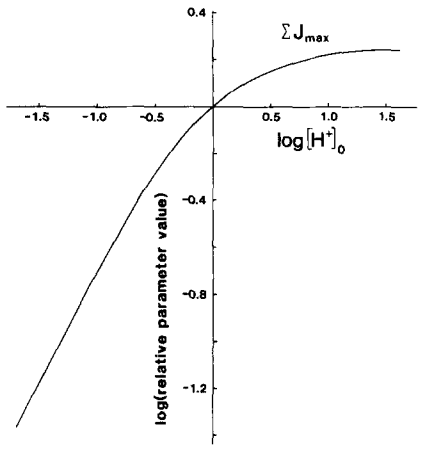

Fig. 12. Response of the isotopic solute flux at saturating $[S]_o$ to variation in $[H^+]_o$ for dual isotherm kinetics: RB^- model. ΣJ_{max} calculated as $J^I_{max} + J^{II}_{max}$ from Fig. 11. All conditions as in Fig. 10

The sum of J^I_{max} and J^{II}_{max}, ΣJ_{max}, is plotted in Fig. 12, also as a function of $[H^+]_o$. As with the RB^+ model, there is a tendency for ΣJ_{max} to saturate at $[H^+]_o$ below that at which J^I_{max} saturates. However, there is one important difference between the behavior of the two models: ΣJ_{max} is not a Michaelian function of $[H^+]_o$ in the case of the RB^- model. This can be confirmed with reference to Table 4. The ratio AB/DE which defines ΣJ_{max} contains in the numerator first- and second-order terms for $[H^+]_o$, and zero-, first- and second-order terms exist in the denominator. Thus the form of the relationship is that of Eq. (3), and Michaelis-Menten kinetics, although possible, do not constitute a unique response.

c. Response to change in $[H^+]_i$. One noteworthy feature of the definitions in Table 4 concerns the absence of the reaction constant k_{75}. This constant is missing because the reaction k_{78} is very fast for the RB^- model at saturating $\Delta\psi$ and N_7 is effectively reduced to 0. Each coefficient A through G in Table 4 therefore consists of zero- and first-order terms for $[H^+]_i$, and there are no second-order terms.

The effects of $[H^+]_i$ on the Michaelis parameters of the RB^- model in the dual isotherm mode contrast strongly with those of the RB^+ model. Given that all the coefficients exhibit first-order dependence on $[H^+]_i$ at high $[H^+]_i$, it might be expected that the Michaelis parameters saturate as $[H^+]_i$ is raised, and this indeed is the case (Fig. 13). The effects of $[H^+]_i$ are small when compared with the $RB+$ model (note difference in ordinate scales in Figs. 9 and 13) because at very negative $\Delta\psi$ the ability of H^+_i to attract more carrier sites to the

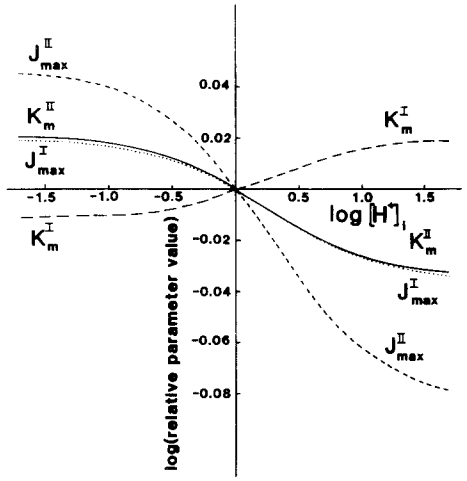

Fig. 13. Effect of $[H^+]_i$ on Michaelis parameters for dual isotherm kinetics: RB^- model. Reference conditions are those of Fig. 10, with $[H^+]_i = 1$ ($k_{75} = k_{31} = 1.0$) and absolute values of rate constants and the Michaelis parameters at $[H^+]_i = 1$ as in the legend of Fig. 10. Michaelis parameters calculated for each $[H^+]_i$ after evaluation of the coefficients in Table 4 and substitution of the coefficients into Eqs. (11)–(14)

inside of the membrane is restricted in the RB^- model. For the particular numerical conditions chosen, the effects of $[H^+]_i$ are predominantly on the J_{max} of the high capacity Michaelean component.

III. Experimental Application

One very clear property of random binding schemes which explain dual isotherms is that as pH is lowered to levels below the pK_a for H^+ binding, so the J_{max} for the low affinity system will disappear. To a large extent, this disappearance is compensated for by an increase in J_{max} associated with the high affinity isotherm. As a result, the sum of the J_{max}'s should remain relatively constant over a range of pH's, although the relative contributions of the high and low affinity components will appear to be pH_o-dependent.

There are few data concerning pH effects on dual isotherms in plants which permit these predictions to be examined properly in the light of previous experiments. However, one system for which a great deal of elegant kinetic information has been collected is the H^+/sugar transport system of *Chlorella*. Komor and Tanner (1975) have shown that 6-deoxyglucose transport in *Chlorella* exhibits biphasic kinetics with respect to external sugar concentration, but that this behavior is marked only when external pH is in the region of neutrality (6.9–7.2). Below this range (pH 6.1), the kinetic characteristics are dominated by the high affinity "system," while above it (pH 8.4), the low affinity "system" dominates. Nevertheless, as the pH is raised from 6.1 to 7.2, ΣJ_{max} decreases by only 10%. At pH 8.4, the decline in ΣJ_{max} is more marked (33% compared with pH 6.1).

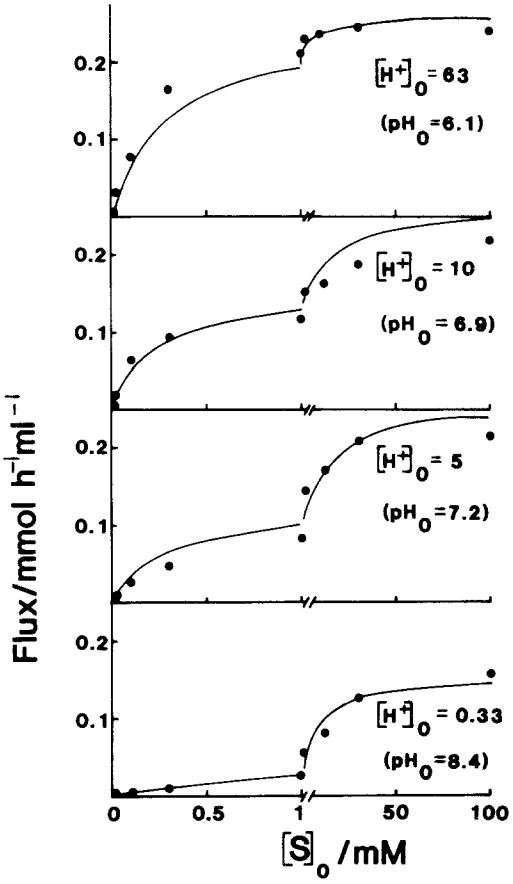

Fig. 14. Ability of random binding model to account for dual isotherm kinetics of sugar transport in *Chlorella*. Experimental points (●) for uptake of 6-deoxyglucose by *Chlorella* from Komor and Tanner (1975), with fits generated by RB^+ model, simplified for very negative $\Delta\psi$ and $[S]_i = 0$. Values of rate constants are excactly those used in Figs. 5–7, i.e., all rate constants were set to unity except $k_{68} = k^o_{86} = k^o_{84} = k_{48} = 0.1$. Thus for the four different pH_o's, the respective values of k_{84} and k_{62} are (top to bottom in figure): 6.3, 63; 1, 10; 0.5, 5; 0.033, 0.33. $[S]_o$ was manipulated as k_{86} and k_{42}. Values for the coefficients in Table 3 were then calculated and these substituted into Eq. (3) for the theoretical fits of the data. Values of Michaelis parameters are as follows:

Relative $[H^+]_o$	K^I_m (mM)	K^{II}_m (mM)	J^I_{max} (mmol h^{-1} ml^{-1})	J^{II}_{max}
63	0.254	70.84	0.242	0.030
10	0.196	17.77	0.151	0.114
5	0.166	12.68	0.104	0.155
0.33	0.106	6.09	0.011	0.139

The kinetic response to pH of sugar transport in *Chlorella* seems therefore to possess exactly those characteristics which are predicted by the random binding of H^+ and sugar to the carrier. Figure 14 shows conventional "dual isotherm" plots for uptake of S at the four relative values of $[H^+]_o$ used by Komor and Tanner. The RB^+ model used to construct these plots is the same as that used for Figs. 5–9, i.e., the only assumptions made are that $\Delta\psi$ is highly negative, that $[S]_i = 0$ and that $k^o_{86} = k_{68} = k^o_{84} = k_{48} = 0.1$, with all other reaction constants = 1. The resemblance to the original plots for sugar transport in *Chlorella* is striking. The change in ΣJ_{max} over the pH range 6.1–7.2 is 7%, while at pH 8.4 it is 45% compared with pH 6.1. The relative values of the flux at $[S]_o = 1$ compared with $[S]_o = 100$ are, for the original data and the model, respectively: pH 6.1: 0.86, 0.75; pH 6.9: 0.54, 0.52; pH 7.2: 0.40, 0.41; pH 8.4: 0.17, 0.20. In conclusion, then, random binding of sugar and H^+ provides a good explanation of the occurrence of biphasic kinetics for sugar uptake in *Chlorella*. Further tests and experimental applications of random binding models are considered in the Discussion.

Discussion

I. Discrimination between Random Binding Models and Other Kinetic Schemes

A. *Slip*

One notion that has been popularly invoked to explain biphasic kinetics is "slip," in which the membrane is assumed to be permeable to the carrier-substrate binary complex as well as to the ternary (H^+-bound) form (e.g. Komor & Tanner, 1975). The low affinity "system" is therefore taken to represent entry of S unaccompanied by H^+, the high affinity "system" being generated by true H^+-S cotransport. Slip has several attractive features. It explains why H^+/S stoichiometry (n) appears to decrease at high external pH, and also provides a ready explanation for the failure of the transmembrane electrochemical gradient of cotransported substrate to come to equilibrium with the protonmotive force, despite the existence of a steady state (Eddy, 1980).

Nevertheless, there are several objections to the generality of slip models as an explanation for these observations, as well as for biphasic kinetics. First, as alluded to in the Introduction, biphasic kinetics have been observed even in cases where the low affinity system generates net solute transport **against** the prevailing electrochemical gradient of S (Sanders, 1984). Second, as we have already shown (Sanders et al., 1984), transinhibition can generate a quasi-steady state far from the region of equilibrium between electrochemical gradients of S and H^+: the effect can occur in transport systems not exhibiting slip.

How, then, might the apparent decline in H^+/S stoichiometry at high external pH be accounted for in terms of the random binding model, which envisages a fixed value of n for the system? The origins of the experimental observation could well reside in the increased ability at high external pH of the primary H^+ efflux pump to compensate for cotransport-associated H^+ entry. This argument is strongly supported by work on H^+/glucose cotransport in *Neurospora*. There, ^{14}C-sugar uptake **and** current (proportional to H^+ flux) through the cotransport system are relatively unaffected over an external pH range in which cotransport-associated H^+ entry (as measured with an external pH electrode) is strongly pH_o-dependent (D. Sanders, K.E. Allen & C.L. Slayman, *in preparation*). In other systems, too, it is well known that unless primary H^+ pumping is inhibited, cotransport-associated H^+ uptake is difficult to detect (e.g. West & Mitchell, 1973).

These observations highlight a fundamental area in which slip models for solute entry can be discriminated from random binding models. Slip requires for neutral solutes that cotransport-dependent membrane current falls in parallel with apparent net H^+ flux through the transport system as pH_o rises, with an increased proportion of solute flux occurring independently of membrane current changes at high pH_o or high $[S]_o$. In contrast, random binding predicts that even in the range of low affinity uptake (high pH_o, high $[S]_o$), a stoichiometric ratio is maintained between net S entry and S-dependent membrane current (although net H^+ influx may well decline as primary H^+ efflux pumping increases).

B. *Ordered Binding*

The present work is an extension of our previous kinetic analysis of ordered binding models (Sanders et al., 1984). Which class of model represents a suitable starting point for analysis of typical cotransport kinetic data? Biphasic kinetic data will clearly fall outside the realm of description by ordered binding models, since ordered binding always generates monophasic Michaelis-Menten kinetics for uptake of isotopic S, irrespective of any other kinetic characteristics of the carrier. In many cases, however, transport can be described as monophasic over a range of conditions, and analysis should therefore begin by application of the model which involves fewest assumptions. The criteria for "fewest assumptions" is to a certain extent a matter of personal preference. Ordered binding models begin with the constraint that steric attributes of the carrier can prevent random addition of ligands, but

the resulting rate equations are relatively simple. While random binding models certainly do not include this steric constraint, their greater topological complexity results in an inherent ability to describe a wider variety of kinetic data. Thus, it might be argued that if data are reasonably well described by ordered binding models, there is no justification for extension of the analysis to systems involving yet more carrier states. However, it should be borne in mind that ordered binding systems are merely sub-classes of more generalized random binding schemes.

C. *Substrate Effects on Membrane Potential*

In most cases of cotransport, the reversal potential of the system is sufficiently far removed from the resting membrane potential to render the solute flux insensitive to changes in $\Delta\psi$. Nevertheless, it is clear that where $[S]_o$ itself substantially affects $\Delta\psi$, the possibility of a significant influence of $\Delta\psi$ on the kinetics of transport should be taken into account. Gerson and Poole (1971) have modelled dual isotherms for anion transport in plants according to the effects of anion concentration on a Goldman diffusion regime. Similarly, the involvement of $\Delta\psi$ appears to be a likely determinant of the effects of external pH on K^+ influx in plants (*cf.* Fried & Noggle, 1958).

D. *More than One Transport System*

An alternative explanation for biphasic kinetics is to suppose that separate carrier systems are responsible for each phase. For sugar transport in *Chlorella*, this explanation appears unlikely because the two kinetic phases appear to behave interdependently as pH_o is varied. Similarly, van Bel et al. (1982) have presented evidence, based on the parallel response of the two phases to a range of treatments, that biphasic uptake of valine in *Commelina* is mediated by a single carrier system. *Neurospora*, though, displays high affinity glucose uptake only after starvation of glucose, the low affinity system being constitutive (Schneider & Wiley, 1971). Furthermore, only high affinity uptake carries electrical current (Slayman & Slayman, 1974), which is strongly suggestive of separate system.

Kinetic analysis with random binding models can give clues to the presence of more than one transport system if, for example, there is failure to observe monophasic kinetics at saturating $[H^+]_o$. *Cis*-(substrate) inhibition kinetics, on the other hand, are diagnostic of a single system (Borst-Pauwels, 1973; Fig. 4). Ideally, genetic and/or reconstitution techniques should be employed in individual cases to generate a more definitive answer to the question of multiple systems.

II. Determination of Reaction Constants

Ordinarily, for studies on intact cells, there will be insufficient data to permit evaluation of all rate constants in a random binding carrier scheme. However, estimates can still be obtained for those rate constants involving binding of ligands externally. The method is to subsume all inaccessible rate constants into a single gross reaction constant (e.g. from state 1 to state 8 in Fig. 1). It has then to be recognized that all rate constants derived from curve fits based on such a model implicitly contain reserve factors which have the capacity to change both the absolute and the relative values of the experimentally-derived rate constants (Hansen et al., 1981).

Certain systems (internally perfused cells and membrane vesicles) also facilitate experimental control of medium composition on both sides of the membrane, and this should extend the range of accessible rate constants. Since the full model contains no fewer than 10 pairs of reaction constants, the range of experimental conditions investigated has to be large. Ideally, the concentration of each ligand should be varied at a series of fixed concentrations of the other ligands in otherwise constant conditions.

The final assignment of rate constants in the above cases will normally be obtained from curve-fitting in which certain key reaction constants are permitted to vary with ligand concentration, the remainder being held constant. There are, however, implicit uncertainities in the method, since the confidence limits for each rate constant, particularly as a function of each of the other rate constants, is not easy to determine. Judicious choice of conditions may nevertheless permit the experimenter to determine certain rate constants more unambiguously. For example, Eqs. (30) and (31) show that for the RB^+ model with $[S]_i = 0$ and $\Delta\psi$ very negative, the ratio J_{stim}/K_{stim} simplifies to Nk^o_{62}. A similar relationship has been pointed out by us previously [Eq. (20) in Sanders et al., 1984)].

III. Site of Charge Translocation

Figures 9 and 13 display a marked contrast in the effects of $[H^+]_i$ on the J_{max}'s for solute transport. For $[S]_i = 0$ and $\Delta\psi$ very negative, the RB^+ model predicts both J_{max}'s fall eventually to zero as $[H^+]_i$ is raised. There are relatively small effects on the K_m's (noncompetitive inhibition). In identical conditions, the RB^- model predicts a decline in both J_{max}'s to stable values at high $[H^+]_i$. This conclusion is a general one, and not restricted to the particular rate constants chosen for the modelling in Figs. 9 and 13: the expression AB/DE ($=\Sigma J_{max}$) exhibits re-

ciprocal dependence on $[H^+]_i$ for the RB^+ model at high $[H^+]_i$ (Table 3) but is independent of $[H^+]_i$ for the RB^- model (Table 4). Thus, provided there is experimental access to the inner compartment, there is a ready basis for determination of the site of charge translocation from isotope studies.

IV. Extension of Random Binding Models

A. *Stoichiometric Ratio Greater than 1*

It has been assumed throughout the present treatment that the H^+/S stoichiometry (n) = 1. While a stoichiometry of $\leqq 1$ is almost certainly valid for some systems (including the lactose/H^+ symporter of *E. coli*: Wright & Overath, 1984), there are many clear-cut examples in the literature of cases in which $n > 1$ (Sanders, 1984). This is particularly true of some anion uptake systems, which generate inward currents even in the case of divalent ions such as SO_4^{2-} for which $n \geqq 3$ (Lass & Ullrich-Eberius, 1984). If all H^+ binding sites are taken as identical, then there exist $n + 1$ possible random binding sequences at each membrane surface and, by implication, $n + 1$ different apparent K_m's. SO_4^{2-} uptake in barley can be described as the sum of three separate kinetic "phases": two Michaelean and one linear (Borstlap, 1981). These kinetics might therefore easily be accommodated by a random binding model for $3H^+/SO_4^{2-}$ cotransport (although noncarrier-mediated diffusion is not ruled out for the linear phase).

B. *Counter Transport*

The present model is as equally applicable to counter-transport as to cotransport systems. There are several examples of counter transport in the membranes of energy-transducing organelles (e.g. Flügge, Gerber & Heldt, 1983) and other endomembranes (e.g. Thom & Komor, 1984). To modify the model it is merely necessary to stipulate that release of effluxed solute can occur either before or after binding of the solute to be influxed.

V. General Conclusions

Random binding schemes for cotransport are capable of describing biphasic kinetics for solute flux, including a commonly observed phenomenon in plant tissues in which a high K_m is associated with a high value of J_{max}, and a low K_m is associated with a lower value of J_{max}. Despite the complexity of the underlying rate equation which describe uptake of isotopic solute by a random-binding carrier, several clear, *testable,* predictions emerge:

(i) The kinetics of S uptake should become monophasic as $[H^+]_o$ is raised to saturating levels. In cases where the initial kinetics are clearly biphasic ($J^{II}_{max} > J^{I}_{max}$, $K^{II}_m \gg K^{I}_m$), the net effect of raising $[H^+]_o$ to a saturating value is a progressive decrease in J^{II}_{max} and a progressive increase in K^{II}_m.
(ii) At saturating $[H^+]_o$, increase in $[S]_i$ should exert uncompetitive inhibition on the influx of S.
(iii) The model predicts proportionality between $[S]_o$ and membrane current for all $[S]_o$, whereas slip and leak models for biphasic kinetics predict a gradually increasing ratio between J_S and current as $[S]_o$ rises.
(iv) The form of carrier which translocates charge can be determined from steady-state kinetic data at negative saturation of $\Delta\psi$ and $[S]_i = 0$. For the case in which positive charge is translocated on the loaded form of the carrier ΣJ_{max} should show reciprocal decline with $[H^+]_i$, whereas for negative charge translocation on the unloaded carrier, ΣJ_{max} becomes independent of $[H^+]_i$, even at very high $[H^+]_i$.

I am indebted to Dr. Rob Brooker for persuading me that analysis of random binding models would be a fruitful exercise, and to Marcelle Sanders for pointing out some of the fundamental algebraic relationships. Thanks are also due to Mick Hopgood for drawing the figures. Financial support was provided by the Agricultural and Food Research Council (U.K.).

References

Bange, G.G.J. 1979. Multiphasic kinetics in solute absorption: An intrinsic property of the transport system? *Z. Pflanzenphysiol.* **91:**75–77

Bel, A.J.E. van, Borstlap, A.C., Pinxteren-Bazuine, A. van, Ammerlaan, A. 1982. Analysis of valine uptake by *Commelina* mesophyll cells in a biphasic active and a diffusional component. *Planta* **155:**335–341

Borstlap, A.C. 1977. Kinetics of the uptake of some neutral amino acids by *Spirodela polyrhiza*. *Acta Bot. Neerl.* **26:**115–128

Borstlap, A.C. 1981. Invalidity of the concept of multiphasic ion absorption in plants. *Plant Cell Environ.* **4:**189–195

Borstlap, A.C. 1983. The use of model-fitting in the interpretation of "dual" uptake isotherms. *Plant Cell Environ.* **6:**407–416

Borst-Pauwels, G.W.F.H. 1973. Two site-single carrier transport kinetics. *J. Theor. Biol.* **40:**19–31

Eddy, A.A. 1978. Proton-dependent solute transport in microorganisms. *In:* Current Topics in Membranes and Transport. F. Bronner and A. Kleinzeller, editors. Vol. 10, pp. 279–360. Academic, New York

Eddy, A.A. 1980. Slip and leak models of gradient-coupled transport. *Trans. Biochem. Soc. London* **8:**271–273

Ehwald, R., Meshcheryakov, A.B., Kholodova, V.P. 1979. Hexose uptake by storage parenchyma of potato and sugar beet at different concentrations and different thicknesses of tissue slices. *Plant Sci. Lett.* **16:**181–188

Epstein, E. 1976. Kinetics of ion transport and the carrier concept. *In:* Encyclopedia of Plant Physiology. M.G. Pitman and U. Lüttge, editors. Vol. 2, Part B, Tissues and Organs. pp. 74–90. Springer-Verlag, Berlin

Epstein, E., Rains, D.W., Elzam, O.E. 1963. Resolution of dual mechanisms of potassium absorption by barley roots. *Proc. Natl. Acad. Sci. USA* **53:**1320–1324

Felle, H. 1981. Stereospecificity and electrogenicity of amino acid transport in *Riccia fluitans*. *Planta* **152:**505–512

Flügge, U.I., Gerber, J., Heldt, H.W. 1983. Regulation of the reconstituted chloroplast phosphate translocator by an H^+ gradient. *Biochim. Biophys. Acta* **725:**229–237

Fried, M., Noggle, J.C. 1958. Multiple site uptake of individual cations by roots as affected by hydrogen ion. *Plant Physiol.* **33:**139–144

Gerson, D.F., Poole, R.J. 1971. Anion absorption by plants. A unary interpretation of dual mechanisms. *Plant Physiol.* **48:**509–511

Gerson, D.F., Poole, R.J. 1972. Chloride accumulation by mung bean root tips. A low affinity active transport system at the plasmalemma. *Plant Physiol.* **50:**603–607

Hansen, U.-P., Gradmann, D., Sanders, D., Slayman, C.L. 1981. Interpretation of current-voltage relationships for "active" ion transport systems: I. Steady-state reaction-kinetic analysis of class-I mechanisms. *J. Membrane Biol.* **63:**165–190

Hansen, U.-P., Slayman, C.L. 1978. Current-voltage relationships for a clearly electrogenic cotransport system. *In:* Membrane Transport Processes. J.F. Hoffman, editor. Vol. 1, pp. 141–154. Raven, New York

Heinz, E., Geck, P., Wilbrandt, W. 1972. Coupling in secondary active transport. Activation of transport by cotransport and/or countertransport with the fluxes of other solutes. *Biochim. Biophys. Acta* **255:**442–461

Kannan, S. 1971. Plasmalemma: The seat of dual mechanisms of ion absorption in *Chlorella pyrenoidosa*. *Science* **173:**927–929

King, E.L., Altman, C. 1956. A schematic method of deriving the rate laws for enzyme-catalysed reactions. *J. Phys. Chem.* **60:**1375–1378

Komor, E., Tanner, W. 1974. The hexose-proton cotransport system of *Chlorella*. pH-dependent change in K_m values and translocation constants of the uptake system. *J. Gen. Physiol.* **64:**568–581

Komor, E., Tanner, W. 1975. Simulation of a high- and low-affinity sugar-uptake system in *Chlorella* by a pH-dependent change in the K_m of the uptake system. *Planta* **123:**195–198

Kotyk, A. 1983. Coupling of secondary active transport with $\Delta\bar{\mu}_{H^+}$. *J. Bioenerg. Biomembr.* **15:**307–319

Lass, B., Ullrich-Eberius, C.I. 1984. Evidence for proton/sulfate cotransport and its kinetics in *Lemna gibba* G1. *Planta* **161:**53–60

Laties, G.G. 1969. Dual mechanisms of salt uptake in relation to compartmentation and long-distance transport. *Annu. Rev. Plant Physiol.* **20:**89–116

McDaniel, C.N., Lyons, R.A., Blackman, M.S. 1981. Amino acid transport in suspension-cultured plant cells: IV. Biphasic saturable uptake kinetics of L-leucine in isolates from six *Nicotiana tabacum* plants. *Plant. Sci. Lett.* **23:**17–23

Mettler, I.J., Leonard, R.T. 1979. Ion transport in isolated protoplasts from tobacco suspension cells: II. Selectivity and kinetics. *Plant Physiol.* **63:**191–194

Niemietz, C., Höfer, M. 1984. Transport of an anionic substrate by the H^+/monosaccharide symport in *Rhodotorula gracilis:* Only the protonated form of the carrier is catalytically active. *J. Membrane Biol.* **80:**235–242

Nissen, P. 1974. Uptake mechanisms: Inorganic and organic. *Annu. Rev. Plant Physiol.* **25:**53–79

Page, M.G.P., West, I.C. 1981. The kinetics of the β-galactoside-proton symport of *Escherichia coli*. *Biochem. J.* **196:**721–731

Pall, M.L. 1971. Amino acid transport in *Neurospora crassa:* IV. Properties and regulation of a methionine transport system. *Biochim. Biophys. Acta* **233:**201–214

Plowman, K.M. 1972. Enzyme Kinetics. McGraw-Hill, New York

Poole, R. 1978. Energy coupling for membrane transport. *Annu. Rev. Plant Physiol.* **29:**437–460

Rybová, R., Nešpürková, L., Janáček, K., Stružinský, R. 1982. Sulphate-uptake isotherm of the alga *Hydrodictyon reticulatum*. *Stud. Biophys.* **92:**123–126

Sabater, B. 1982. A mechanism for multiphasic uptake of solutes in plants. *Physiol. Plant.* **55:**121–128

Sanders, D. 1980. Control of Cl^- influx in *Chara* by cytoplasmic Cl^- concentration. *J. Membrane. Biol.* **52:**51–60

Sanders, D. 1984. Gradient-coupled chloride transport in plant cells. *In:* Chloride Transport Coupling in Biological Membranes and Epithelia. G.A. Gerencser, editor. pp. 63–120. Elsevier, Amsterdam

Sanders, D., Hansen, U.-P. 1981. Mechanism of Cl^- transport at the plasma membrane of *Chara corallina:* II. Transinhibition and the determination of H^+/Cl^- binding order from a reaction kinetic model. *J. Membrane Biol.* **58:**139–153

Sanders, D., Hansen, U.-P., Gradmann, D., Slayman, C.L. 1984. Generalized kinetic analysis of ion-driven cotransport systems: A unified interpretation of selective ionic effects on Michaelis parameters. *J. Membrane Biol.* **77:**123–152

Sanders, D., Slayman, C.L. 1983. A simple origin for "dual isotherms," based on H^+ cotransport. *Plant Physiol.* **72 Suppl.:**140

Sanders, D., Slayman, C.L., Pall, M.L. 1983. Stoichiometry of H^+/amino acid cotransport in *Neurospora crassa* revealed by current-voltage analysis. *Biochim. Biophys. Acta* **735:**67–76

Schneider, R.P., Wiley, W.R. 1971. Kinetic characteristics of the two glucose transport systems in *Neurospora crassa*. *J. Bacteriol.* **106:**479–486

Schultz, S.G., Curran, P. 1970. Coupled transport of sodium and organic solutes. *Physiol. Rev.* **50:**637–718

Segel, I.H. 1975. Enzyme Kinetics. Wiley & Sons, New York

Slayman, C.L., Slayman, C.W. 1974. Depolarization of the plasma membrane of *Neurospora* during active transport of glucose: Evidence for a proton-dependent cotransport system. *Proc. Natl. Acad. Sci. USA* **71:**1935–1939

Thom, M., Komor, E. 1984. H^+-sugar antiport as the mechanism of sugar uptake by sugarcane vacuoles. *FEBS Lett.* **173:**1–4

Turner, R.J. 1981. Kinetic analysis of a family of cotransport models. *Biochim. Biophys. Acta* **649:**269–280

West, I.C. 1980. Energy coupling in secondary active transport. *Biochim. Biophys. Acta* **604:**91–126

West, I.C., Mitchell, P. 1973. Stoichiometry of lactose-H^+ symport across the plasma membrane of *Escherichia coli*. *Biochem. J.* **132:**587–592

Wright, J.K., Overath, P. 1984. Purification of the lactose : H^+ carrier of *Escherichia coli* and characterization of galactoside binding and transport. *Eur. J. Biochem.* **138:**497–508

Received 15 August 1985

Appendix I

Derivation of the Complete Rate Equation for Isotopic Flux through a Random Binding Cotransport System

The generalized random binding carrier is shown in Fig. 15A. The derivation of the rate equation to express movement of isotopically labeled solute ($^*S$) from the outside to the inside begins by assuming that $[^*S]_i = 0$. (Unlabeled S may nevertheless be present inside.) The flux of labeled solute, $^*J_S$, is then given as

$$^*J_S = {}^*N_1k_{15} + {}^*N_3k_{37} \tag{A1}$$

in which $^*N_j$ is the concentration of isotopically labeled carrier state j.

The proportion of carrier states 1 and 3 that is isotopically labeled is not immediately known. For purposes of calculation of isotopic flux it is therefore easier to express Eq. (A1) in terms of carrier states not bound to isotope, i.e., the carrier states 4 and 8 to which $^*S$ binds. The following rate equations are therefore solved for N_4 and N_8:

$$\frac{d^*N_3}{dt} = 0 = {}^*N_1k_{13} - {}^*N_3(k_{37} + k_{31}) \tag{A2}$$

$$\frac{d^*N_1}{dt} = 0 = {}^*N_2k_{21} + {}^*N_3k_{31} - {}^*N_1(k_{12} + k_{13} + k_{15}) \tag{A3}$$

$$\frac{d^*N_2}{dt} = 0 = {}^*N_1k_{12} + N_4k_{42} + {}^*N_6k_{62} - {}^*N_2(k_{21} + k_{24} + k_{26}) \tag{A4}$$

$$\frac{d^*N_6}{dt} = 0 = {}^*N_2k_{26} + N_8k_{86} - {}^*N_6(k_{62} + k_{68}). \tag{A5}$$

Equations (A2) through (A5) explicitly recognize that the carrier state distribution will be in a steady state during measurement of isotopic flux. Substitution of these equations into Eq. (A1) leads to

$$J_s = \frac{S_o k_{21}\alpha[N_4k_{42}^o(k_{62} + k_{68}) + N_8k_{86}^ok_{62}]}{\alpha[(k_{62} + k_{68})(k_{21} + k_{24}) + k_{68}k_{26}] + k_{12}\{(k_{37} + k_{31})[k_{24}(k_{62} + k_{68}) + k_{68}k_{26}]\}} \tag{A6}$$

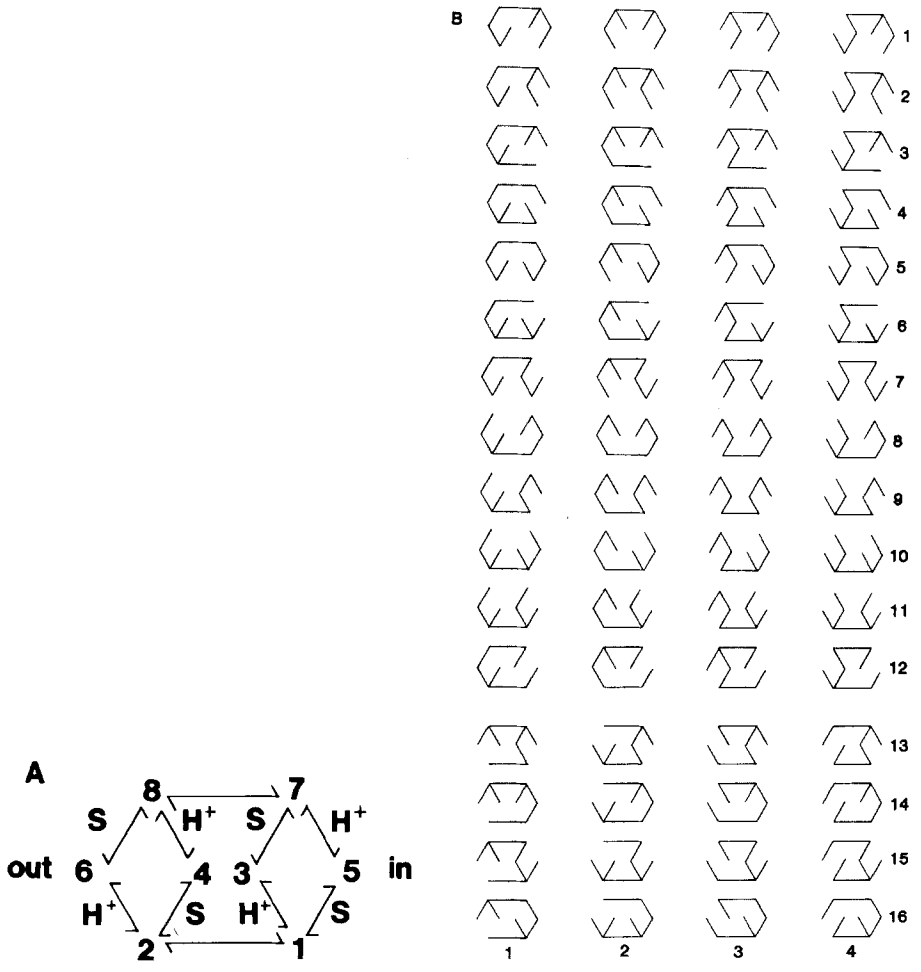

Fig. 15. (*A*) Generalized diagram for random-binding cotransport system, based on Fig. 1. (*B*) King & Altman diagrams for the reaction scheme in *A*. For explanation, *see* text

with

$$\alpha = k_{15}(k_{37} + k_{31}) + k_{13}k_{37} \tag{A7}$$

and S_o, the concentration of solute externally. (The * notation has been dropped, since all external solute is labeled at known specific activity.)

It simply remains, then, to express the concentration of the carrier states N_4 and N_8 in terms of the rate constants of the carrier cycle. This is accomplished by the King & Altman method (King & Altman, 1956; *see also* Plowman, 1972; Segel, 1975). Figure 15*B* shows the 64 King & Altman diagrams for the reaction scheme in Fig. 15*A*. Each diagram can be related to any of the eight states as the product of the seven rate constants directed towards that state. The carrier-state concentration or density, N_j, can then be expressed as a proportion of the total carrier concentration, N, by the ratio of the 64 King & Altman diagrams relating to state j and the 512 diagrams describing all eight states. We can express this as

$$\frac{N_j}{N} = \frac{64KA_j}{512KA_T}. \tag{A8}$$

For the purposes of an initial rate measurement, N can be taken as constant, and for the numerical analysis in this paper, N is set to unity.

Table A1 gives the numbers of King & Altman diagrams subsuming S_o-dependent terms for each of the eight states. Thus, extracting k_{42} and k_{86} from the King & Altman terms and denoting the residual expression as KA_j^o (six rate constants left in each diagram after extraction of k_{42} or k_{86}) or KA_j^{oo} (five rate constants left after extraction of k_{42} and k_{86})

$$J_s = N \cdot \frac{\begin{array}{r} S_o k_{21}\alpha[Sk_{42}^o k_{86}^o(12KA_4^o(k_{62} + k_{68}) + 20KA_8^o k_{62}) \\ + 52KA_4 k_{42}^o(k_{62} + k_{68}) + 44KA_8 k_{86}^o k_{62}] \end{array}}{\begin{array}{r} \mathrm{DEN}[S_o^2(12KA_T^{oo}k_{42}^o k_{86}^o) + S_o(172KA_T^o k_{42}^o \\ + 76KA_T^o k_{86}^o) + 212KA_T] \end{array}} \tag{A9}$$

where DEN is the denominator of Eq. (A6).

Equation (A9) can therefore be written as Eq. (3), with the identify of the coefficients in Table 1 defined by straightforward term-by-term comparison.

Equation (A9) can also, of course, be rewritten to make explicit terms for any of the other three ligands: H_o^+, S_i and H_i^+. However, our practice in the rest of the paper has been to identify the presence of ligand binding terms in each of the S_o-dependent coefficients in Eq. (A9).

Table A1. Distribution of King & Altman terms subsuming $[S]_o$ among expressions for carrier states

Carrier state	Number of terms subsuming		
	$S_o^2 k_{42}^o k_{86}^o$	$S_o k_{42}^o$	$S_o k_{86}^o$
1	8	28	8
2	12	32	12
3	6	26	6
4	0	0	12
5	6	26	6
6	16	16	28
7	4	24	4
8	0	20	0

Appendix II

Table A2*a*. Expansion of King & Altman terms for the condition of saturating $[H^+]_o$

	From Eq. (22) (*B*) $12KA_4^{oo}$			From Eq. (23) (*C*) $16KA_4^{oo}$			From Eq. (27) (*G*) $16KA_T^{oo}$		
	State	Column	Row	State	Column	Row	State	Column	Row
$k_{24}k_{15}k_{57}k_{37}k_{78}$	4	1	1	4	4	1	4	4	1
$+k_{24}k_{13}k_{57}k_{37}k_{78}$			2			2			2
$+k_{24}k_{12}k_{57}k_{37}k_{78}$			3			3			3
$+k_{24}k_{12}k_{31}k_{57}k_{78}$			4			4			4
$+k_{24}k_{31}k_{15}k_{57}k_{78}$			5			5			5
$+k_{24}k_{12}k_{31}k_{51}k_{78}$			6			6			6
$+k_{24}k_{51}k_{13}k_{37}k_{78}$			7			7			7
$+k_{24}k_{51}k_{37}k_{75}k_{12}$			8			8			8
$+k_{24}k_{57}k_{73}k_{31}k_{12}$			9			9			9
$+k_{24}k_{75}k_{51}k_{31}k_{12}$			10			10			10
$+k_{24}k_{73}k_{31}k_{51}k_{12}$			11			11			11
$+k_{24}k_{12}k_{51}k_{37}k_{78}$			12			12			12
Extracted:	$[H^+]_o k_{62}^o$, $[S]_o k_{86}^o$ $4KA_8^{oo}$			$[H^+]_o k_{62}^o$, $[H^+]_o k_{84}^o$			$[H^+]_o k_{62}^o$, $[H^+]_o k_{84}^o$		
$+k_{21}k_{13}k_{37}k_{57}k_{78}$	8	2	13	4	3	13	4	3	13
$+k_{21}k_{15}k_{37}k_{57}k_{78}$			14			14			14
$+k_{21}k_{51}k_{13}k_{37}k_{78}$			15			15			15
$+k_{21}k_{31}k_{15}k_{57}k_{78}$			16			16			16
Extracted:	$[H^+]_o k_{62}^o$, $[S]_o k_{42}^o$			$[H^+]_o k_{62}^o$, $[H^+]_o k_{84}^o$			$[H^+]_o k_{62}^o$, $[H^+]_o k_{84}^o$		

Table A2*b*. Expansion of King & Altman terms for the condition of saturating $[H^+]_o$

	From Eq. (25) (*E*) $36KA_T^{ooo}$			From Eq. (26) (*F*) $36KA_T^{ooo}$		
	State	Column	Row	State	Column	Row
$k_{21}k_{37}k_{57}k_{78}$	1	1	3	1	4	3
$+k_{21}k_{31}k_{57}k_{78}$			4			4
$+k_{21}k_{31}k_{51}k_{78}$			6			6
$+k_{21}k_{37}k_{75}k_{51}$			8			8
$+k_{21}k_{57}k_{73}k_{31}$			9			9
$+k_{21}k_{75}k_{51}k_{31}$			10			10
$+k_{21}k_{73}k_{51}k_{31}$			11			11
$+k_{21}k_{51}k_{37}k_{78}$			12			12
$+k_{15}k_{57}k_{37}k_{78}$	2	1	1	2	4	1
$+k_{13}k_{57}k_{37}k_{78}$			2			2
$+k_{12}k_{57}k_{37}k_{78}$			3			3
$+k_{12}k_{31}k_{57}k_{78}$			4			4
$+k_{31}k_{15}k_{57}k_{78}$			5			5
$+k_{12}k_{31}k_{51}k_{78}$			6			6
$+k_{51}k_{13}k_{37}k_{78}$			7			7
$+k_{51}k_{37}k_{75}k_{12}$			8			8
$+k_{57}k_{73}k_{31}k_{12}$			9			9
$+k_{75}k_{51}k_{31}k_{12}$			10			10
$+k_{73}k_{31}k_{51}k_{12}$			11			11
$+k_{12}k_{51}k_{37}k_{78}$			12			12
$+k_{57}k_{78}k_{21}k_{13}$	3	1	4	3	4	4
$+k_{78}k_{21}k_{51}k_{13}$			6			6
$+k_{21}k_{15}k_{57}k_{73}$			8			8
$+k_{21}k_{13}k_{57}k_{73}$			9			9
$+k_{21}k_{13}k_{75}k_{51}$			10			10
$+k_{21}k_{13}k_{51}k_{73}$			11			11
$+k_{78}k_{21}k_{31}k_{15}$	5	1	6	5	4	6
$+k_{21}k_{15}k_{37}k_{75}$			8			8
$+k_{21}k_{13}k_{37}k_{75}$			9			9
$+k_{21}k_{31}k_{15}k_{75}$			10			10
$+k_{21}k_{73}k_{31}k_{15}$			11			11
$+k_{37}k_{78}k_{21}k_{15}$			12			12
$+k_{21}k_{15}k_{57}k_{37}$	7	1	8	7	4	8
$+k_{21}k_{13}k_{37}k_{57}$			9			9
$+k_{21}k_{31}k_{15}k_{57}$			10			10
$+k_{21}k_{51}k_{13}k_{37}$			11			11
Extracted: $[H^+]_o k_{62}^o$, $[S]_o k_{86}^o$, $[S]_o k_{42}^o$;				$[H^+]_o k_{62}^o$, $[H^+]_o k_{84}^o$, $[S]_o k_{42}^o$		

Expansion of King & Altman Terms for the Condition of Saturating $[H^+]_o$

The complete expansion of the King & Altman terms in Eqs. (22), (23) and (25)–(27) is given in Tables A2*a* and A2*b* in such a way as to show the fundamental similarities between the coefficients *B*, *C* and *G*, on one hand, and *E* and *F*, on the other. The numbers to the right of the table are to enable easy identification of the appropriate King & Altman diagrams from Fig. 15. The "extracted" terms appear in the original equations.

Appendix III

Derivation of Equations for the Simplified Models, with $[S]_i = 0$ and $\Delta\psi$ Very Negative

Table A3, column 1, shows for each of the carrier states the number of King & Altman terms remaining (from the original total of 64: Fig. 15*B*) after imposing the simplifying condition of $[S]_i = 0$. Columns 2 and 3 show respectively for the RB^+ and RB^- models the number of terms present after the additional restriction of very negative $\Delta\psi$ is imposed. The King & Altman terms appear explicitly in the coefficient definitions in Tables 3 and 4.

Table A3. Distribution of King & Altman terms among carrier states after simplification of random binding model

Carrier state	Number of terms remaining with		
	$k_{73} = k_{51} = 0$	$k_{73} = k_{51} = k_{12} = 0$ and k_{21} large	$k_{73} = k_{51} = k_{87} = 0$ and k_{78} large
1	8	8	8
2	20	0	20
3	4	4	4
4	26	6	26
5	52	32	8
6	26	6	26
7	44	24	0
8	32	12	32